Quaternary Science Reviews 185 (2018) 9–26

Contents lists available at ScienceDirect

Quaternary Science Reviews

journal homepage: www.elsevier.com/locate/quascirev

The MIS 3 maximum of the Torres del Paine and Última Esperanza ice lobes in Patagonia and the pacing of southern mountain glaciation

Juan-Luis García [a, *], Andrew S. Hein [b], Steven A. Binnie [c], Gabriel A. Gómez [a, d], Mauricio A. González [a], Tibor J. Dunai [c]

[a] Instituto de Geografía, Facultad de Historia, Geografía y Ciencia Política, Pontificia Universidad Católica de Chile, Avenida Vicuña Mackenna 4860, Macul, Santiago 782-0436, Chile
[b] School of GeoSciences, University of Edinburgh, Edinburgh, Scotland EH8 9XP, UK
[c] Institut für Geologie und Mineralogie, Universität zu Köln, Zülpicher Str. 49b, 50674 Köln, Germany
[d] Instituto de Ciencias de la Tierra, Universidad Austral de Chile, Valdivia, Chile

ARTICLE INFO

Article history:
Received 1 October 2017
Received in revised form
21 January 2018
Accepted 22 January 2018
Available online 7 February 2018

ABSTRACT

The timing, structure and termination of the last southern mountain glaciation and its forcing remains unclear. Most studies have focused on the global Last Glacial Maximum (LGM; 26.5–19 ka) time period, which is just part of the extensive time-frame within the last glacial period, including Marine Isotope Stages 3 and 4. Understanding the glacial fluctuations throughout the glacial period is a prerequisite for uncovering the cause and climate mechanism driving southern glaciation and the interhemispheric linkages of climate change. Here, we present an extensive (n = 65) cosmogenic ^{10}Be glacier chronology derived from moraine belts marking the pre-global LGM extent of the former Patagonian Ice Sheet in southernmost South America. Our results show the mountain ice sheet reached its maximum extent at 48.0 ± 1.8 ka during the local LGM, but attained just half this extent at 21.5 ± 1.8 ka during the global LGM. This finding, supported by nearby glacier chronologies, indicates that at orbital time scales, the southern mid-latitude glaciers fluctuated out-of-phase with northern hemisphere ice sheets. At millennial time-scales, our data suggest that Patagonian and New Zealand glaciers advanced in unison with cold Antarctic stadials and reductions in Southern Ocean sea surface temperatures. This implies a southern middle latitudes-wide millennial rhythm of climate change throughout the last glacial period linked to the north Atlantic by the bipolar seesaw. We suggest that winter insolation, acting alongside other drivers such as the strength and/or position of the southern westerlies, controlled the extents of major southern mountain glaciers such as those in southernmost South America.

1. Introduction

Variations in Earth's orbital parameters control the geographic and seasonal distribution of incoming solar radiation and this plays a primary role in the pacing of ice ages (Milankovitch, 1941). Nonetheless, we lack a thorough knowledge of the timing, structure and termination of the last glaciation in southern hemisphere mountains and the mechanisms forcing change. While southern mountain glaciers expanded during the global Last Glacial Maximum (gLGM) (e.g., Mix et al., 2001, 26.5–19 ka), the timing of their maximum extent (or local Last Glacial Maximum, lLGM) is rarely known because terminal moraines have remained mostly undated. An increasing number of recent studies suggest extended southern mid-latitude glaciers earlier than the gLGM (e.g., Doughty et al., 2015; Darvill et al., 2015a; Schaefer et al., 2015; Kelley et al., 2014; Putnam et al., 2013; Sagredo et al., 2011). Most of the available data is from New Zealand and very limited pre-gLGM paleoclimate records, including Marine Isotope Stage (MIS) 3 and 4, exist for Southern South America that can be linked to local or global climate controls (Jouzel et al., 2007; Huybers and Denton, 2008; WAIS Divide Project Members, 2015). Therefore, the timing of the lLGM for southern mountain glaciers and relevant forcing mechanisms still need to be defined, with consequences for our understanding of the interhemispheric phasing of maximum glaciation (Broecker and Denton, 1989; McCulloch et al., 2005; Huybers and Denton, 2008; Denton et al., 1999; Kaplan et al., 2008a; Hein

* Corresponding author.
E-mail address: jgarciab@uc.cl (J.-L. García).

https://doi.org/10.1016/j.quascirev.2018.01.013
0277-3791/

et al., 2010; Putnam et al., 2013; Doughty et al., 2015; Darvill et al., 2015a, 2016). For instance, globally-distributed ice and marine sediment cores indicate near synchrony of past climate changes at the orbital time scale (10^{4-5} years) (Jouzel et al., 2007; Lisiecki and Raymo, 2005), but the question of whether northern ice sheets and southern mountain glaciers reached their maximum extents in-phase within the last glacial period remains unresolved (Gillespie and Molnar, 1995; Hughes et al., 2013; Mercer, 1984; Sugden et al., 2005). Here we present new geochronological data that gives insights into the timing and structure of the last glaciation in southern South America. Our data derive from 65 cosmogenic ^{10}Be exposure ages sampled from boulders on three moraine belts deposited by the Torres del Paine ice lobe and two moraine belts deposited by the Última Esperanza ice lobe (Fig. 1) in southern Patagonia (50-51°S).

2. Regional setting

The former Patagonian ice sheet (PIS) extended along the temperate southern Andes between 38 and 56°S (Hollin and Schilling, 1981; Caldenius, 1932; Glasser et al., 2008, Fig. 2A). During the LGM, the PIS was drained by fast-flowing outlet glaciers that followed ice streams further upglacier (Glasser and Jansson, 2005). Nonetheless, important differences existed between the southern and northern sections of the PIS. For instance, the northern PIS can be regarded as a mountain style of glaciation whereas the southern PIS as a mountain ice sheet style of glaciation (García, 2012). In the Chilean Lake District (39–41 °S, Fig. 1), glaciers were relatively thin, steep, narrow and short when compared to the thicker and larger ice that mantled southernmost South America (50–55 °S). Here, extensive, low-gradient ice lobes extended between about 100 and 200 km from the mountain ice catchments (e.g., García et al., 2014; Darvill et al., 2015b, 2017; Bendle et al., 2017a,b). The former Torres del Paine and Última Esperanza ice lobes drained a southeast section of the PIS in southernmost South America and extended 100 km further east of the present-day ice field.

The region occupies an isolated and unique geographic position

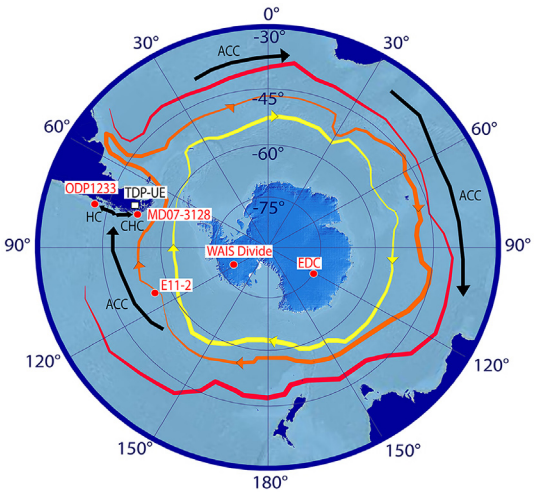

Fig. 1. Location of the former Torres del Paine (TDP) and Última Esperanza (UE) ice lobes in Southernmost South America from an Antarctic and Southern Ocean perspective. Colored lines represent approximate location of ocean fronts (red: Subtropical Front; orange: Sub-Antarctic Front; yellow: Polar Front; based on Gersonde et al. (2005). Marine and ice core records discussed in the paper are shown. EDC: Epica Dome C ice core, WAIS Divide: West Antarctic Ice Sheet Divide ice core, ACC: Antarctic Circumpolar Current; CHC: Cape Horn Current; HC: Humboldt Current. (For interpretation of the references to color in this figure legend, the reader is referred to the Web version of this article.)

given that no other continental mass exists at these latitudes. Today, the climate in the region is temperate-cold, with a significant precipitation gradient across the Andes Mountains. Westerly wind-transported storms originating at the Antarctic Polar Front Zone are associated with elevated precipitation levels (c. 6–10 m per year at present day ice fields, DGA, 1987; Escobar et al., 1992) and decreased temperatures (Garreaud, 2007) that directly affect local climate and the ice fields mass balance (e.g., Rivera et al., 2002). Cloudiness and precipitation occur year-round over the ice fields, at the former catchments of the Torres del Paine and Última Esperanza ice lobes (Miller, 1976; Warren and Sugden, 1993; Carrasco et al., 2002). To the east, precipitation reduces rapidly in just a few tens of km to only a few hundred mm per year within the rain shadow of the Andes, where a forest-steppe ecotone occurs (Moreno et al., 2009). Distant from the North Atlantic climate, the southern part of the former PIS is expected to preserve a morpho-stratigraphic record of climate change highlighting any prominent paleoclimate signal from the adjacent Antarctic and Southern Ocean realm (Fig. 1).

In this study, we have mapped and dated, from oldest to youngest, the Río de las Vizcachas (RV) I, RV II, and Torres del Paine (TDP) I moraines in Torres del Paine, and the Río Turbio (RT) and Arauco (AR) moraine belts in Última Esperanza (Caldenius, 1932; Meglioli, 1992; Marden and Clapperton, 1995; Sagredo et al., 2011; García et al., 2014; Darvill et al., 2014, 2017) (Fig. 2). The RV I and RT moraines are the most extensive, having been deposited ~100 km to the east of the present-day South Patagonian Ice Field. The RV II and AR frontal moraines occur just inboard of the outermost moraines. The TDP I moraine, on the other hand, occurs ~50 km inboard of the outermost RV I moraine, reflecting a far less-extensive glacial phase for which there is no equivalent preserved in the Última Esperanza valley (Fig. 2).

3. MATERIALS and methods

3.1. Sample collection

In situ-produced ^{10}Be exposure ages were measured in rocks collected using a hammer and chisel from the upper ~2 cm of tall (wherever possible >100 cm height) well-preserved boulders of quartz-bearing lithologies (e.g., Michel et al., 2008) embedded in, or resting on stable moraine crest tops (Figs. 3–4). Two cobbles were sampled from the proglacial RV outwash plain (Torres del Paine), but we did not include them in the calculations of moraine ages because this landform may have been reworked during multiple RV glacial oscillations. In the field, we used a hand-held GNSS systems to measure geographic position (accurate to within approximately <5 m; vertical error ≤10 m). We determined the shielding effect of the surrounding relief using clinometer readings at 15° intervals. Dip angle and dip direction of the sampled surfaces were recorded and these data were used to correct the exposure-age calculations when sampled surfaces dipped >10°, which occurred rarely.

3.1.1. Torres del Paine ice lobe ^{10}Be samples

In Torres del Paine we collected samples from the RV I, RV II and TDP I moraines (Fig. 3). Most of the RV I samples (>75%) were obtained from the northern lateral moraine at Sierra Contreras. All of these samples were granite in lithology and for the most part (>75%) taller than 100 cm. Boulders were randomly distributed over the broad and convex crest of the moraine. We sampled boulders along the central axis of the crest but also the upper proximal and distal slopes (~<20°) where necessary. Two samples were collected at the southern RV I lateral (RVILS-12-01, RVILS-12-02) and another two boulders (RVI-08-01, RVI-08-01) were collected at the outer frontal RV I moraine. Finally, two cobbles

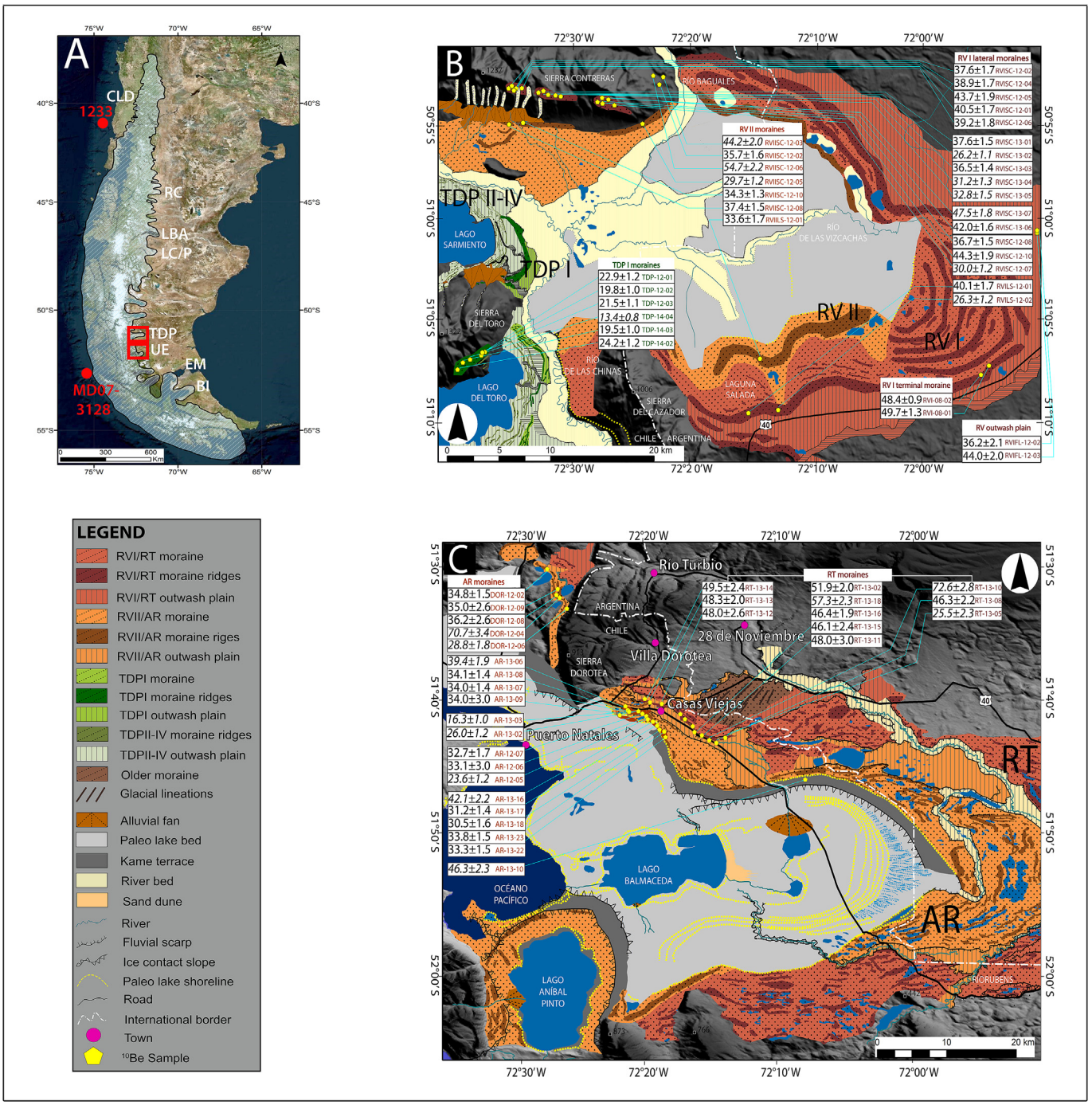

Fig. 2. Glacial geomorphology of the Torres del Paine and Última Esperanza ice lobes. (A) Approximate extent of the PIS during the LGM after Hollin and Schilling (1981), Caldenius (1932) and Glasser et al. (2008). CLD: Chilean Lake District; RC: Río Cisnes; LBA: Lago Buenos Aires; LC/LP: Lago Cochrane/Lago Pueyrredón; TDP: Torres del Paine; UE: Última Esperanza; EM: Estrecho de Magallanes; BI: Bahía Inútil. Off-shore sediment cores discussed in the paper are shown also **(B)** Torres del Paine and **(C)** Última Esperanza geomorphological maps depict, among other geomorphic features, the moraine belts mapped and dated within this paper. From oldest to youngest, these moraine belts are the Río de las Vizcachas (RV) I, RV II, and Torres del Paine (TDP) I moraines from the Torres del Paine site, and the Río Turbio (RT) and Arauco (AR) moraine belts from the Última Esperanza site. Boxes include ^{10}Be exposure ages in ka (black) and sample numbers (color follows the associated moraine belt). Samples in italics were rejected as outliers and not included in the discussion. (For interpretation of the references to color in this figure legend, the reader is referred to the Web version of this article.)

were sampled from the outwash plain grading from the frontal RV moraine complex. These are RVIFL-12-02, RVIFL-12-03 (Fig. 2B).

Six of the seven boulders collected from the RV II moraine were obtained from the northern lateral moraine at Sierra Contreras (Fig. 2B). The RV II moraine is parallel to the RV I moraine but it does not contain as many boulders on its surface. Sampled boulders ranged from 74 to 112 cm tall and were collected from stable moraine tops. At the Laguna Salada area, we sampled a single boulder (no more found) from the outermost lateral moraine (RVIILS- 12-01) (Fig. 2B).

At the inboard northern lateral TDP I moraine we sampled six boulders, most of them of granitic lithology. Samples were for the most part <100 cm tall and distributed along the 1 km-long lateral moraine.

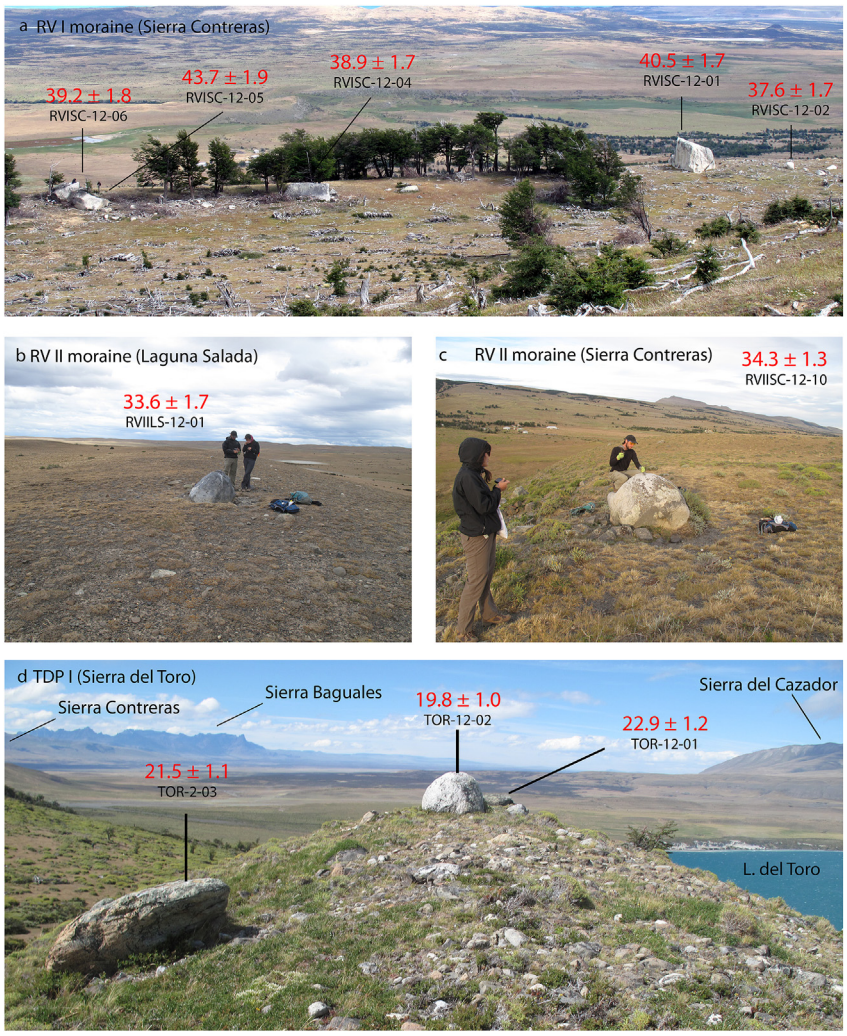

Fig. 3. Example of sampled boulders and their cosmogenic ^{10}Be exposure ages at Torres del Paine.

3.1.2. *Última Esperanza ice lobe ^{10}Be samples*

At the Última Esperanza ice lobe we sampled boulders from the RT and AR moraine belts. Samples were obtained from the northern lateral moraines, including the Sierra Dorotea site (Sagredo et al., 2011; Figs. 2C and 4). The RT moraine is continuous and exposes distinct inner, intermediate and outer ridges, containing sparsely distributed surface boulders. The moraine belt can reach 1000 m wide and it is delimited to the north by older (outer) drumlinised landforms, and to the south by the Arauco outwash plain. We obtained 11 samples along ~5 km of the RT moraine. Two of the 11 sampled boulders were >100 cm tall; the other sampled boulders ranged from 49 to 88 cm above the ground. Sampled boulders included quartz-bearing lithologies, such as granites, occurring on top of the close-spaced gentle moraine ridges making-up the RT landform (Fig. 4).

At the inner AR moraine belt we collected rock samples from the outermost moraine but also from inboard ridges at several locations along this landform. We sampled boulders along the length of the lateral moraine complex. For the most part, AR samples come from a ~6 km range along the AR moraine between the *Villa Dorotea* and *Casas Viejas* international roads (Fig. 2C). Another cluster of samples was collected at the Sierra Dorotea (the DOR samples). Sampled boulders ranged from 51 to 343 cm tall (Fig. 4).

3.2. *Sample preparation and analysis*

All samples were crushed, sieved and separated with heavy liquids in the Catholic University laboratory facilities (Santiago). Quartz isolation was done at the University of Edinburgh and the University of Cologne using acid etching techniques described by Kohl and Nishiizumi (1992), with modifications at Edinburgh following Bierman et al. (2002) and at Cologne following Mifsud et al. (2013). Samples obtained at Torres del Paine (RV and TDP moraines) were prepared as Accelerator Mass Spectrometry (AMS) targets at the University of Cologne. At the University of Edinburgh, we prepared samples from the Última Esperanza basin: the RT and AR moraines.

At the University of Edinburgh's cosmogenic nuclide laboratory, 5–27 g of pure quartz separate were spiked with ~250 μg ^{9}Be carrier (Scharlau Beryllium ICP standard solution, 1000 mg/l, density 1.02 g/ml) and prepared as AMS targets using standard techniques outlined in Hein (2009). Reagent blanks (n = 5) prepared alongside the samples, gave ^{10}Be/^{9}Be values between ~1×10^{-15} to ~4×10^{-15}.

For samples prepared in the University of Cologne cosmogenic nuclide target preparation laboratory we used the multiple-column 'standard techniques' outlined in Binnie et al. (2015). Following purity checks on an assay of the samples by ICP-OES, between ~5

Fig. 4. Example of sampled boulders and their cosmogenic ^{10}Be exposure ages at Última Esperanza.

and 35 g of pure quartz separate was spiked with ~300 μg of commercially available Be carrier (Scharlau, 1000 mg/l, Beryllium ICP standard solution density 1.02 g/ml). Reagent blanks (n = 7) prepared alongside the samples, gave ^{10}Be/^{9}Be values between ~6×10^{-16} to ~7×10^{-15}.

Measurements of ^{10}Be/^{9}Be were undertaken at CologneAMS (Dewald et al., 2013), normalized to the revised standard values reported by Nishiizumi et al. (2007). Two samples, RVI-08-01 and RVI-08-02, were prepared at Lamont-Doherty Earth Observatory and their ^{10}Be/^{9}Be measurements were undertaken at the AMS facility at Lawrence Livermore National Laboratory. The analytical data, including reagent blank-corrected ^{10}Be concentrations, is presented in Table 1.

The final ^{10}Be concentration in Table 1 is reported following subtraction of the ^{10}Be atoms measured in the respective blanks. Blank subtractions constituted between <1 and <5% of the total ^{10}Be atoms measured in the samples, except for the younger Torres del Paine moraine samples, where the largest subtraction was ~8% of the total. The analytical uncertainties for the ^{10}Be concentrations were determined by summing in quadrature the uncertainties in the mass of ^{9}Be added during sample processing (estimated as 1% at 1σ in both Edinburgh and Cologne) and the AMS measurement uncertainties of both the sample and blank.

3.3. Data interpretation

The glacier history reconstruction presented in this paper derives from interpretations of both geomorphology and cosmogenic ^{10}Be exposure ages. While the ^{10}Be ages likely represent the timing of moraine abandonment, within given uncertainties, we consider them to represent the culmination of the respective glacial advance. For calculation of ^{10}Be ages we assumed zero erosion and used the CRONUS online exposure-age calculator Version 2.2 and Version 2.2.1 of the constants file (Balco et al., 2008) applying the local ^{10}Be production rate site in Southern Patagonia (3.71 ± 0.11 atoms^{-1} g^{-1} yr^{-1}; Kaplan et al., 2011). Selecting the scheme of Dunai (2001) or Lal (1991) and Stone (2000) or Desilets and Zreda (2003) for scaling ^{10}Be measurements to sea-level and high-latitude provide age-differences within 1% (e.g., within the analytical uncertainties). The scaling method by Pigati and Lifton (2004), Lifton et al. (2008, 2014) produces c. 2% younger ages. In this study, we use Dunai (2001) but this choice does not change our conclusions. The inputs used in the CRONUS online calculator are given in Table 1 and resulting ^{10}Be ages are displayed in Table 2.

In order to calculate the age of a glacial advance, we separated the ^{10}Be ages based on moraine belts. Each of these landforms can include multiple ridges from where we sampled rocks for ^{10}Be dating (Fig. 2). We first obtained the summed probability distribution for each moraine belt (Figs. 5–6). Visual inspection and reduced chi-square values for each moraine reveals that the data do not conform to a normal distribution and so we prefer to use the more robust median and associated median absolute deviation (MAD), instead of the mean and standard deviation statistics that are used preferentially when data is normally distributed (Rock et al., 1987). The median and the MAD together strengthen the central trend of the data, which reflects the peak age of the

Table 1
Analytical data from ^{10}Be samples at the Torres del Paine ice lobe and Última Esperanza ice lobe.

SAMPLE ID	Lat °S	Long °W	Elevation (m a.s.l.)	Sample thickness (cm)	Boulder height (cm)	Shielding correction	^{10}Be ±1σ (10^4 atoms g^{-1})	^{10}Be/^{9}Be ratio ± 1σ	^{10}Be Standarization
Río de las Vizcachas_RV I Terminal Moraine									
RVI-08-01	−51,1057	−71,8733	330	0,7	50	1000	28.49 ± 0.72	1.85E-13 ± 4.68E-15	07KNSTD
RVI-08-02	−51,0993	−71,8686	312	0,9	123	1000	27.29 ± 0.35	1.88E-13 ± 3.69E-15	07KNSTD
Río de las Vizcachas_RV I Lateral Moraine									
RVISC-13-07	−50,9131	−72,4447	652	2,1	177	0,999	36.54 ± 1.38	3.68E-13 ± 1.33E-14	07KNSTD
RVISC-12-10	−50,9090	−72,5224	711	0,9	74	1000	35.60 ± 1.47	1.35E-13 ± 5.27E-15	07KNSTD
RVISC-12-05	−50,9067	−72,5482	731	0,8	248	1000	36.45 ± 1.57	2.02E-13 ± 8.29E-15	07KNSTD
RVISC-13-06	−50,9139	−72,4358	656	1,4	180	0,997	32.59 ± 1.23	3.23E-13 ± 1.16E-14	07KNSTD
RVISC-12-01	−50,9064	−72,5498	731	4,4	610	0,999	32.85 ± 1.30	2.93E-13 ± 1.11E-14	07KNSTD
RVILS-12-01	−51,1591	−72,2347	450	1,1	100	0,999	26.17 ± 1.06	2.15E-13 ± 8.10E-15	07KNSTD
RVISC-12-06	−50,9067	−72,5482	731	0,9	236	0,999	32.70 ± 1.46	3.19E-13 ± 1.38E-14	07KNSTD
RVISC-12-02	−50,9063	−72,5500	732	3,1	115	0,999	30.22 ± 1.36	1.32E-13 ± 5.69E-15	07KNSTD
RVISC-12-04	−50,9065	−72,5492	736	1,3	218	1000	31.88 ± 1.33	1.44E-13 ± 5.69E-15	07KNSTD
RVISC-13-01	−50,9084	−72,5335	720	1,7	242	1000	30.84 ± 1.18	3.67E-13 ± 1.34E-14	07KNSTD
RVISC-12-08	−50,9092	−72,5243	701	1,3	103	1000	29.15 ± 1.20	1.29E-13 ± 4.99E-15	07KNSTD
RVISC-13-03	−50,9087	−72,5292	710	1,5	82	0,999	29.71 ± 1.12	3.07E-13 ± 1.11E-14	07KNSTD
RVISC -13-05	−50,9095	−72,5200	707	1,7	101	1000	26.61 ± 1.22	2.69E-13 ± 1.19E-14	07KNSTD
RVISC -13-04	−50,9092	−72,5240	706	1,8	91	1000	25.25 ± 1.00	2.90E-13 ± 1.09E-14	07KNSTD
RVISC -12-07	−50,9099	−72,5164	700	0,8	129	1000	23.90 ± 0.93	2.22E-13 ± 9.21E-15	07KNSTD
RVILS -12-02	−51,1567	−72,1999	456	1,5	112	0,998	17.15 ± 0.76	2.03E-13 ± 8.77E-15	07KNSTD
RVISC-13-02	−50,9088	−72,5313	711	1,6	58	1000	21.36 ± 0.89	2.19E-13 ± 9.71E-15	07KNSTD
Río de las Vizcachas_RV II Moraine									
RVIISC-12-06	−50,8954	−72,3644	340	0,6	105	1000	32.13 ± 1.26	3.49E-13 ± 1.32E-14	07KNSTD
RVIISC-12-03	−50,8980	−72,3548	326	1,1	74	0,996	26.09 ± 1.14	2.45E-13 ± 1.04E-14	07KNSTD
RVIISC-12-08	−50,9285	−72,5823	382	1,7	88	0,999	22.68 ± 0.86	2.95E-13 ± 1.04E-14	07KNSTD
RVIISC-12-02	−50,8995	−72,3593	354	0,9	112	1000	21.28 ± 0.92	1.89E-13 ± 7.61E-15	07KNSTD
RVIISC-12-10	−50,9277	−72,5670	386	0,7	101	1000	21.07 ± 0.81	2.50E-13 ± 8.97E-15	07KNSTD
RVIILS-12-01	−51,1153	−72,2248	328	2,7	100	0,998	19.28 ± 0.94	2.05E-13 ± 9.69E-15	07KNSTD
RVIISC-12-05	−50,9202	−72,3825	333	0,9	76	0,999	17.35 ± 0.71	1.94E-13 ± 7.31E-15	07KNSTD
RV Outwatsh Plain									
RVIFL-12-03	−51,0406	−71,8089	292	1,99	10	1000	24.68 ± 1.11	1.95E-13 ± 8.40E-15	07KNSTD
RVIFL-12-02	−51,0408	−71,8092	295	1,56	9	0,996	20.33 ± 1.15	5.86E-14 ± 3.10E-15	07KNSTD
Torres del Paine_TDP I Moraine									
TOR-14-02	−51,1261	−72,6095	274	2,2	22	0,995	13.24 ± 0.62	1.71E-13 ± 7.64E-15	07KNSTD
TOR-12-01	−51,1222	−72,6008	271	1,1	81	0,999	12.66 ± 0.64	1.16E-13 ± 5.56E-15	07KNSTD
TOR-12-03	−51,1223	−72,6010	274	1,3	69	0,997	11.87 ± 0.58	1.26E-13 ± 5.88E-15	07KNSTD
TOR-12-02	−51,1223	−72,6009	272	1,5	101	0,998	10.89 ± 0.53	1.17E-13 ± 5.40E-15	07KNSTD
TOR-14-03	−51,1243	−72,6056	258	2,6	29	0,996	10.48 ± 0.53	1.63E-13 ± 7.86E-15	07KNSTD
TOR-14-04	−51,1237	−72,6041	270	2,3	17	0,996	7.27 ± 0.43	1.01E-13 ± 5.59E-15	07KNSTD

Table 1 (*continued*)

SAMPLE ID	Lat °S	Long °W	Elevation (m a.s.l.)	Sample thickness (cm)	Boulder height (cm)	Shielding correction	^{10}Be ±1σ (10^4 atoms g^{-1})	^{10}Be/^{9}Be ratio ± 1σ	^{10}Be Standarization
Río Turbio_RT Moraine									
TUR-13-10	−51,7217	−72,2709	277	1,3	58	1000	40.36 ± 1.52	4.27E-13 ± 1.54E-14	07KNSTD
TUR-13-18	−51,7095	−72,2865	269	1,1	49	1000	31.81 ± 1.25	3.00E-13 ± 1.13E-14	07KNSTD
TUR-13-02	−51,7077	−72,2884	252	1,5	74	1000	28.33 ± 1.08	4.70E-13 ± 1.72E-14	07KNSTD
TUR-13-14	−51,6996	−72,3072	251	2,1	88	1000	26.92 ± 1.29	1.63E-13 ± 7.48E-15	07KNSTD
TUR-13-13	−51,6999	−72,3070	251	1,8	152	1000	26.27 ± 1.06	3.78E-13 ± 1.47E-14	07KNSTD
TUR-13-11	−51,7175	−72,2759	271	1,5	119	1000	26.72 ± 1.61	1.27E-13 ± 7.44E-15	07KNSTD
TUR-13-12	−51,7002	−72,3046	248	1,1	69	1000	26.22 ± 1.40	1.37E-13 ± 7.00E-15	07KNSTD
TUR-13-08	−51,7232	−72,2684	255	1,6	54	1000	25.42 ± 1.15	2.49E-13 ± 1.09E-14	07KNSTD
TUR-13-16	−51,7129	−72,2822	272	1,5	84	0,999	25.82 ± 1.05	2.75E-13 ± 1.07E-14	07KNSTD
TUR-13-15	−51,7142	−72,2819	263	1,4	61	1000	25.48 ± 1.31	2.23E-13 ± 1.11E-14	07KNSTD
TUR-13-05	−51,7227	−72,2594	275	1,1	54	1000	14.33 ± 1.26	4.50E-14 ± 3.78E-15	07KNSTD
Arauco_AR Moraine									
DOR-12-04	−51,5576	−72,4630	331	1,6	100	1000	41.11 ± 1.90	2.71E-13 ± 1.21E-14	07KNSTD
AR-13-10	−51,7701	−72,1483	201	0,9	74	1000	24.29 ± 1.18	2.12E-13 ± 9.78E-15	07KNSTD
AR-13-16	−51,70191	−72,3408	227	1,5	90	1000	22.48 ± 1.16	2.42E-13 ± 1.19E-14	07KNSTD
AR-13-06	−51,6837	−72,3808	249	2,1	131	1000	21.37 ± 1.01	3.00E-13 ± 1.36E-14	07KNSTD
DOR-12-08	−51,5585	−72,4677	332	1,8	105	1000	21.19 ± 1.51	1.51E-13 ± 1.05E-14	07KNSTD
DOR-12-09	−51,5514	−72,4650	321	0,9	129	0,999	20.41 ± 1.51	2.46E-13 ± 1.78E-14	07KNSTD
DOR-12-02	−51,5285	−72,4800	300	0,9	131	1000	19.93 ± 0.82	3.02E-13 ± 1.19E-14	07KNSTD
AR-13-08	−51,6901	−72,3745	234	1,4	56	1000	18.36 ± 0.74	2.70E-13 ± 1.03E-14	07KNSTD
AR-13-07	−51,6904	−72,3735	243	2,1	122	0,998	18.30 ± 0.74	2.84E-13 ± 1.08E-14	07KNSTD
AR-13-09	−51,6905	−72,3854	232	1,9	343	1000	18.16 ± 1.55	1.83E-13 ± 1.51E-14	07KNSTD
AR-13-23	−51,7126	−72,3275	226	1,5	51	1000	18.07 ± 1.80	2.51E-13 ± 1.05E-14	07KNSTD
AR-13-22	−51,7166	−72,3251	224	1,1	65	1000	17.82 ± 0.78	2.66E-13 ± 1.10E-14	07KNSTD
AR-12-06	−51,6957	−72,3493	237	0,9	74	1000	17.91 ± 1.58	2.77E-13 ± 2.41E-14	07KNSTD
AR-12-07	−51,6919	−72,3545	248	0,9	222	1000	17.91 ± 1.91	1.29E-13 ± 6.05E-15	07KNSTD
AR-13-17	−51,7036	−72,3387	229	1,4	51	1000	16.73 ± 0.73	2.79E-13 ± 1.16E-14	07KNSTD
AR-13-18	−51,7093	−72,3351	233	2,1	85	1000	16.28 ± 0.83	1.02E-13 ± 4.66E-15	07KNSTD
DOR-12-06	−51,5686	−72,4530	311	1,4	66	0,999	16.57 ± 0.99	9.49E-14 ± 5.40E-15	07KNSTD
AR-13-02	−51,6889	−72,3596	249	1,0	115	1000	14.22 ± 0.64	1.48E-13 ± 6.14E-15	07KNSTD
AR-12-05	−51,6958	−72,3489	233	1,3	123	0,999	12.70 ± 0.61	1.58E-13 ± 7.30E-15	07KNSTD
AR-13-03	−51,6890	−72,3595	249	2,0	52	0,999	88.25 ± 0.52	1.20E-13 ± 6.57E-15	07KNSTD

summed probability that, in our case, best represents the age of the moraine.

We treated samples more than two MADs distant from the median age of the moraine as outliers and did not include them in our calculations. We performed this procedure iteratively until remaining data satisfied this criterion. This approach allows us to aggregate the samples that cluster to form a well-defined peak age, which gives the highest probability for the timing of the moraine abandonment after the glacial advance culmination. Outliers detected and rejected appear in italics in Fig. 2 and Table 2 (see the outlier note in the supplementary information). We present the median age for each moraine, including all filtered samples that produce the main probability peak (see Figs. 5–6). Moraine age uncertainties quoted are the sum of the MAD and the South

Table 2
^{10}Be ages for Torres del Paine ice lobe and Última Esperanza ice lobes.

SAMPLE ID	Du int ext	De int ext	Li int ext	Lm int ext
Río de las Vizcachas_RV I Terminal Moraine				
RVI-08-01	**48600 ± 1300 2100**	48700 ± 1300 2100	47800 ± 1300 2000	49000 ± 1300 2100
RVI-08-02	**47400 ± 1000 1900**	47500 ± 1000 1900	46600 ± 1000 1800	47800 ± 1000 1900
Río de las Vizcachas_RV I Lateral Moraine				
RVISC-13-07	**47500 ± 1800 2400**	47700 ± 1800 2400	46600 ± 1800 2400	47800 ± 1800 2400
RVISC-12-10	**43400 ± 1800 2300**	43600 ± 1800 2300	42600 ± 1800 2300	43700 ± 1800 2400
RVISC-12-05	**43700 ± 1900 2400**	43800 ± 1900 2400	42800 ± 1900 2400	44000 ± 1900 2400
RVISC-13-06	**42000 ± 1600 2100**	42100 ± 1600 2100	41200 ± 1600 2100	42200 ± 1600 2100
RVISC-12-01	**40500 ± 1700 2100**	40600 ± 1700 2100	39700 ± 1700 2100	40800 ± 1700 2100
RVILS-12-01	**40200 ± 1600 2100**	40300 ± 1600 2100	39500 ± 1600 2100	40400 ± 1600 2100
RVISC-12-06	**39200 ± 1800 2200**	39300 ± 1800 2200	38400 ± 1800 2200	39500 ± 1800 2200
RVISC-12-02	**36900 ± 1700 2100**	36900 ± 1700 2100	36200 ± 1700 2100	37000 ± 1700 2100
RVISC-12-04	**38200 ± 1600 2100**	38300 ± 1600 2100	37400 ± 1600 2000	38400 ± 1600 2100
RVISC-13-01	**37600 ± 1500 1900**	37700 ± 1500 1900	36800 ± 1500 1900	37800 ± 1500 1900
RVISC-12-08	**36000 ± 1500 1900**	36100 ± 1500 1900	35300 ± 1500 1900	36200 ± 1500 1900
RVISC-13-03	**36500 ± 1400 1900**	36600 ± 1400 1900	35800 ± 1400 1800	36700 ± 1400 1900
RVISC -13-05	**32800 ± 1500 1900**	32800 ± 1500 1900	32200 ± 1500 1800	33000 ± 1500 1900
RVISC -13-04	**31200 ± 1300 1600**	31200 ± 1300 1600	30600 ± 1300 1600	31400 ± 1300 1600
RVISC -12-07	**29400 ± 1200 1500**	29500 ± 1200 1500	28900 ± 1200 1500	29600 ± 1200 1500
RVILS -12-02	**26300 ± 1200 1500**	26300 ± 1200 1500	26000 ± 1200 1500	26400 ± 1200 1500
RVISC-13-02	**26200 ± 1100 1400**	26300 ± 1100 1400	25800 ± 1100 1400	26400 ± 1100 1400
Río de las Vizcachas_RV II Moraine				
RVIISC-12-06	**54700 ± 2200 2900**	54800 ± 2200 2900	53800 ± 2200 2800	55000 ± 2200 2900
RVIISC-12-03	**45100 ± 2000 2500**	45200 ± 2000 2500	44400 ± 2000 2500	45400 ± 2000 2500
RVIISC-12-08	**37400 ± 1400 1900**	37400 ± 1400 1900	36800 ± 1400 1900	37600 ± 1400 1900
RVIISC-12-02	**35700 ± 1600 2000**	35700 ± 1600 2000	35200 ± 1600 1900	35900 ± 1600 2000
RVIISC-12-10	**34300 ± 1300 1800**	34300 ± 1300 1800	33700 ± 1300 1700	34400 ± 1300 1800
RVIILS-12-01	**33600 ± 1700 2000**	33600 ± 1700 2000	33000 ± 1700 2000	33700 ± 1700 2000
RVIISC-12-05	**29700 ± 1200 1600**	29700 ± 1200 1600	29300 ± 1200 1600	29800 ± 1200 1600
RV Outwatsh Plain				
RVIFL-12-03	**44000 ± 2000 2500**	44100 ± 2000 2500	43300 ± 2000 2500	44400 ± 2000 2500
RVIFL-12-02	**36200 ± 2100 2400**	36200 ± 2100 2400	35700 ± 2100 2400	36400 ± 2100 2400
Torres del Paine_TDP I Moraine				
TOR-14-02	**24200 ± 1200 1400**	24200 ± 1200 1400	23900 ± 1200 1400	24300 ± 1200 1400
TOR-12-01	**22900 ± 1200 1400**	22900 ± 1200 1400	22700 ± 1200 1400	23000 ± 1200 1400
TOR-12-03	**21500 ± 1100 1300**	21500 ± 1100 1300	21300 ± 1100 1300	21600 ± 1100 1300
TOR-12-02	**19800 ± 1000 1200**	19800 ± 1000 1200	19600 ± 1000 1200	19800 ± 1000 1200
TOR-14-03	**19500 ± 1000 1200**	19500 ± 1000 1200	19300 ± 1000 1200	19600 ± 1000 1200
TOR-14-04	**13400 ± 800 900**	13400 ± 800 900	13300 ± 800 900	13400 ± 800 900
Río Turbio_RT Moraine				
RT-13-10	**72600 ± 2800 3700**	72800 ± 2800 3700	71300 ± 2800 3700	73200 ± 2800 3800
RT-13-18	**57300 ± 2300 3000**	57400 ± 2300 3000	56300 ± 2300 3000	57800 ± 2300 3000
RT-13-02	**51900 ± 2000 2700**	52000 ± 2000 2700	51000 ± 2000 2600	52400 ± 2000 2700
RT-13-14	**49500 ± 2400 2900**	49700 ± 2400 2900	48700 ± 2400 2900	50000 ± 2400 3000
RT-13-13	**48300 ± 2000 2600**	48500 ± 2000 2600	47500 ± 2000 2500	48800 ± 2000 2600
RT-13-11	**48000 ± 3000 3400**	48200 ± 3000 3400	47200 ± 3000 3300	48500 ± 3000 3400
RT-13-12	**48000 ± 2600 3100**	48100 ± 2600 3100	47200 ± 2600 3000	48500 ± 2600 3100
RT-13-08	**46300 ± 2200 2600**	46500 ± 2200 2600	45600 ± 2200 2600	46800 ± 2200 2700
RT-13-16	**46400 ± 1900 2500**	46500 ± 1900 2500	45600 ± 1900 2400	46800 ± 1900 2500
RT-13-15	**46100 ± 2400 2900**	46300 ± 2400 2900	45400 ± 2400 2800	46600 ± 2400 2900
RT-13-05	**25500 ± 2300 2400**	25500 ± 2300 2400	25200 ± 2300 2400	25700 ± 2300 2400
Arauco_AR Moraine				
DOR-12-04	**70700 ± 3400 4100**	70800 ± 3400 4100	69400 ± 3400 4000	71200 ± 3400 4100
AR-13-10	**46300 ± 2300 2800**	46400 ± 2300 2800	45600 ± 2300 2700	46800 ± 2300 2800
AR-13-16	**42100 ± 2200 2600**	42200 ± 2200 2600	41400 ± 2200 2600	42500 ± 2200 2600
AR-13-06	**39400 ± 1900 2300**	39500 ± 1900 2300	38800 ± 1900 2300	39800 ± 1900 2300
DOR-12-08	**36200 ± 2600 2900**	36300 ± 2600 2900	35600 ± 2600 2800	36400 ± 2600 2900
DOR-12-09	**35000 ± 2600 2900**	35100 ± 2600 2900	34500 ± 2600 2800	35200 ± 2600 2900
DOR-12-02	**34800 ± 1500 1900**	34900 ± 1500 1900	34300 ± 1500 1800	35000 ± 1500 1900
AR-13-08	**34100 ± 1400 1800**	34200 ± 1400 1800	33600 ± 1400 1800	34400 ± 1400 1800
AR-13-07	**34000 ± 1400 1800**	34000 ± 1400 1800	33500 ± 1400 1800	34200 ± 1400 1800
AR-13-09	**34000 ± 3000 3100**	34000 ± 3000 3100	33400 ± 3000 3100	34200 ± 3000 3200
AR-13-23	**33800 ± 1500 1900**	33900 ± 1500 1900	33300 ± 1500 1900	34100 ± 1500 1900
AR-13-22	**33300 ± 1500 1900**	33300 ± 1500 1900	32800 ± 1500 1800	33600 ± 1500 1900
AR-12-06	**33100 ± 3000 3100**	33100 ± 3000 3100	32600 ± 3000 3100	33300 ± 3000 3200
AR-12-07	**32700 ± 1700 2000**	32800 ± 1700 2000	32200 ± 1700 2000	33000 ± 1700 2000
AR-13-17	**31200 ± 1400 1700**	31200 ± 1400 1700	30800 ± 1400 1700	31500 ± 1400 1700
AR-13-18	**30500 ± 1600 1900**	30500 ± 1600 1900	30000 ± 1600 1900	30700 ± 1600 1900
DOR-12-06	**28800 ± 1800 2000**	28800 ± 1800 2000	28400 ± 1800 2000	29000 ± 1800 2000
AR-13-02	**26000 ± 1200 1500**	26000 ± 1200 1500	25600 ± 1200 1500	26100 ± 1200 1500
AR-12-05	**23600 ± 1200 1400**	23600 ± 1200 1400	23300 ± 1200 1400	23800 ± 1200 1400
AR-13-03	**16300 ± 1000 1100**	16300 ± 1000 1100	16200 ± 1000 1100	16300 ± 1000 1100

Note: ^{10}Be ages in years calculated with four different scaling protocols using the CRONUS online calculator (version 2.2, Balco et al., 2008). 'Du' is the time dependent scaling scheme of Dunai (2001) (highlighted with bold letters; we use this in our study), 'De' the scaling scheme presented in Desilets and Zreda (2003), 'Li' the scaling based on Lifton

et al. (2008) and Pigati and Lifton (2004), and 'Lm' is the time dependent version of Lal/Stone scaling scheme (Stone, 2000; Lal, 1991). All ages were calculated using a ^{10}Be production rate measured at the nearby Lago Argentino area in southern Patagonia (Kaplan et al., 2011), which agrees closely to New Zealand's Macaulay site (Putnam et al., 2010b). In the paper we discuss ages using the Du scaling scheme. Density of rock used for calculating ^{10}Be ages is 2.65 g cm^{-3}. Age uncertainties reported are 1 standard deviation internal (int), which include analytical uncertainty only, and external (ext), which includes systematic uncertainties associated with production rate scaling. Ages have been rounded using three significant figures. Ages in italics are outliers.

Patagonian ^{10}Be production rate uncertainty of 3% (Kaplan et al., 2011).

4. Results

4.1. Torres del Paine ice lobe

4.1.1. Río de las Viscachas (RV) moraines

The mapping of the RV moraine at Torres del Paine has been described in previous studies (Caldenius, 1932; García et al., 2014, Fig. 2B). The eastern frontal margin includes multiple concentric moraine ridges deposited over a distance of c. 15 km. Moraine ridges are wide (e.g., tens of meters) and are difficult to distinguish from the ground. The area is better described as a hummocky terrain including moraine mounds and depressions that form an overall irregular topography. Small, dry lake basins throughout the moraine field separate the moraine mounds, which in turn can reach up to about 30 m tall. Ice marginal meltwater channels help to differentiate each of the RV frontal moraines deposited here.

Two distinct RV I and RV II lateral moraines are well preserved at both sides of the former Torres del Paine ice lobe (García et al., 2014). They are mostly continuous for ~50 km delineating the former extent of the ablation zone of the Torres del Paine ice lobe. At the southern margin, at the Laguna Salada site (Fig. 2B), the RV I and RV II lateral moraines are distinct and appear separated from each other by a mosaic of marginal and subglacial glacial landforms that include subdued moraine ridges, intermoraine depressions occupied by dry lakes, and glacial lineations exposing the former ice flow direction. At the northern margin, the Torres del Paine ice lobe buttressed against the Sierra Contreras mountain and deposited two prominent lateral RV I and RV II moraines, which can be tracked almost continuously for >8 km. Here, both the RV I and RV II landforms occur mostly as broad single moraine crests at ~700 and ~350 m a.s.l., respectively. Most of our RV rock samples were obtained at Sierra Contreras (Figs. 2B–3a, c).

4.1.2. Torres del Paine (TDP) I moraines

Previous studies (Marden and Clapperton, 1995; García et al., 2014) provided a detailed description of this landform. At Lago del Toro, the TDP I occurs as a well-defined moraine belt that can include up to three moraine ridges (Fig. 2B). Although glaciofluvial erosion has breached this landform, we have mapped it to continue up into the southern flank of Sierra del Toro to form a single, sharp (e.g., proximal slopes at the angle of repose), well-preserved lateral moraine. The lateral TDP I moraine ridge is up to several meters across and extends continuously for more that 1 km. Our TOR samples were obtained from this part of the moraine (Fig. 3d).

4.2. Última Esperanza ice lobe

4.2.1. Río Turbio (RT) and Arauco (AR) moraines

Past work (Caldenius, 1932; Meglioli, 1992; Sagredo et al., 2011; Darvill et al., 2014) have provided insight into the main geomorphic attributes of these concentric dual moraine belts. Both moraine arcs are semi-continuous for ~80–100 km surrounding the Lago Balmaceda plane basin (Fig. 2C) and expose the former perimeter of the Última Esperanza ice lobe during the maximum extent attained during the last glacial period.

The terminus of the RT and AR moraines occupy a large area where a mosaic of well developed moraine ridges and irregularly shaped ridges (cf., Darvill et al., 2014) coexist with intermoraine depressions carved by ice marginal meltwater channels. Similar to the RV moraine complex (Torres del Paine ice lobe), the RT and AR frontal moraines were deposited over a distance of ~18 km across an east west transect. Well-developed frontal moraine ridges are not conspicuous and the moraine landscape is better defined as bands of irregularly shaped ridges separated by depressions that help to distinguish the moraines (cf., Darvill et al., 2014). Major ice marginal channels parallel to the former ice snout could hint at the different generations of landforms. As in the Torres del Paine ice lobe, lateral moraines are developed at both sides of the former Última Esperanza ice lobe over a distance of ~50 km. These lateral moraines are better preserved on the northern side where we focused on sampling for our ^{10}Be glacier chronology (Fig. 4). Here, an extensive and continuous outwash corridor, carved during the younger AR glacial advance separates these two generations of moraine belts (Fig. 2C).

The RT lateral moraine complex can include three distinct ridges that make up a distinct drift level ~40 m above the inner AR drift. The moraine ridges are well preserved but are rather wide and low in relief with gentle slopes, exposing a former glacial limit (Fig. 4).

Several ridges make up the inboard AR moraine arc. Whereas the outer moraines within the AR belt are well preserved, the inner ridges can appear subdued and are surrounded by glaciofluvial deposits. For instance, three gentle, wide radii crests are distinct at Sierra Dorotea, but multiple ridges occur in the Casas Viejas area. Intermoraine depressions filled with mires and ponds separate different ridges. The AR moraines can be up to 15 m but normally are <10-5 m tall and continuous for hundreds of meters. Several moraine ridges can converge into one single crest, depicting the composite character of some of these landforms that demark the former maximum AR extent of the Última Esperanza ice lobe. At the northeast margin, the Última Esperanza ice lobe buttressed against the Sierra Dorotea and filled its upper basin to build the AR moraines inboard of the RT moraines. Extensive glaciolacustrine shorelines were eroded on the inner side of the AR moraine belt during deglaciation and reflect the postglacial paleolake history (cf., Sagredo et al., 2011) (Fig. 2C).

4.3. Chronology

At Torres del Paine, the RV moraines were dated at their frontal and lateral outer moraines. Two boulders at the outer frontal RV I moraine yielded a median exposure-age of 48.0 ± 1.6 ka (age range 48.6–47.4 ka), while eleven boulders on the outer lateral portion of the RV I moraine at Sierra Contreras and Laguna Salada yielded a median age of 39.2 ± 2.0 ka (age range 44.3 ka - 36.5 ka). The outer RV II lateral moraines sampled at Sierra Contreras and Laguna Salada yielded a median age of 35.0 ± 1.5 ka (n = 4, age range 33.6 ka – 37.4 ka). Two cobbles collected from the RV outwash plain yielded 44.0 ± 2.0 ka and 36.2 ± 2.1 ka. Finally, the inner TDP I northern lateral moraine yielded median exposure-age of 21.5 ± 1.8 ka (n = 5, age range 19.5 ka – 24.2 ka) (Fig. 8). Despite the relatively small size of the TDP I boulders, we do not see an obvious effect on the exposure ages obtained from them. In fact, excluding TOR-14-04, the exposure ages form a distinct cluster and an overall congruent chronological pattern.

At Última Esperanza, we sampled boulders from the outer

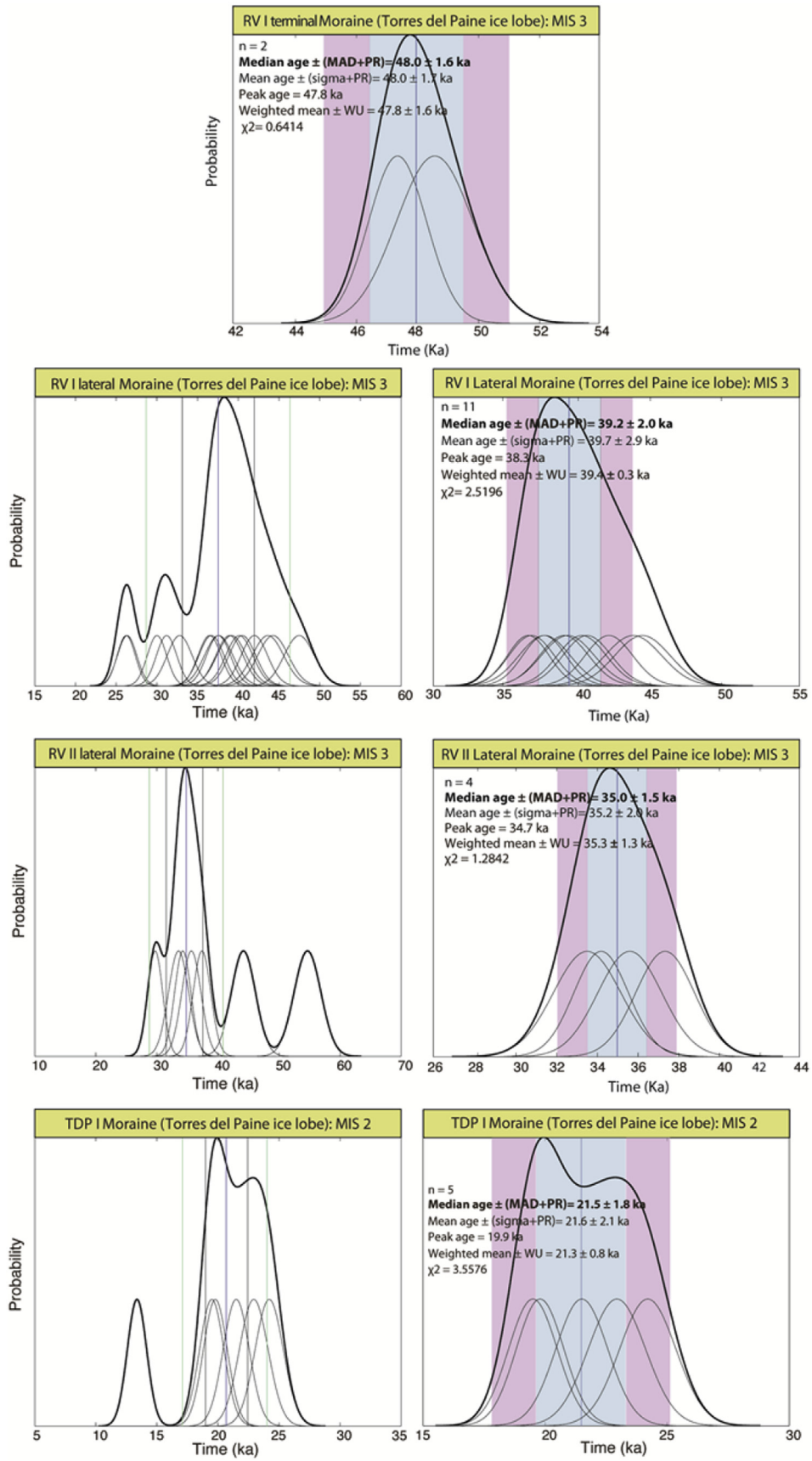

Fig. 5. Probability plots and statistical data for the moraines ^{10}Be dated in this study in Torres del Paine. The left plots include all samples and the right plot shows the filtered dataset (i.e., following rejection of outliers) for each moraine. The black and green vertical lines in the left plots indicate the 1 x MAD and 2 x MAD from the median (blue line), respectively. In the right plots, the vertical blue line represents the median age of the moraine. The light blue and pink vertical bands represent the ±1 and 2 uncertainties (MAD + 3% ^{10}Be production rate), respectively, for the filtered moraine age. (For interpretation of the references to color in this figure legend, the reader is referred to the Web version of this article.)

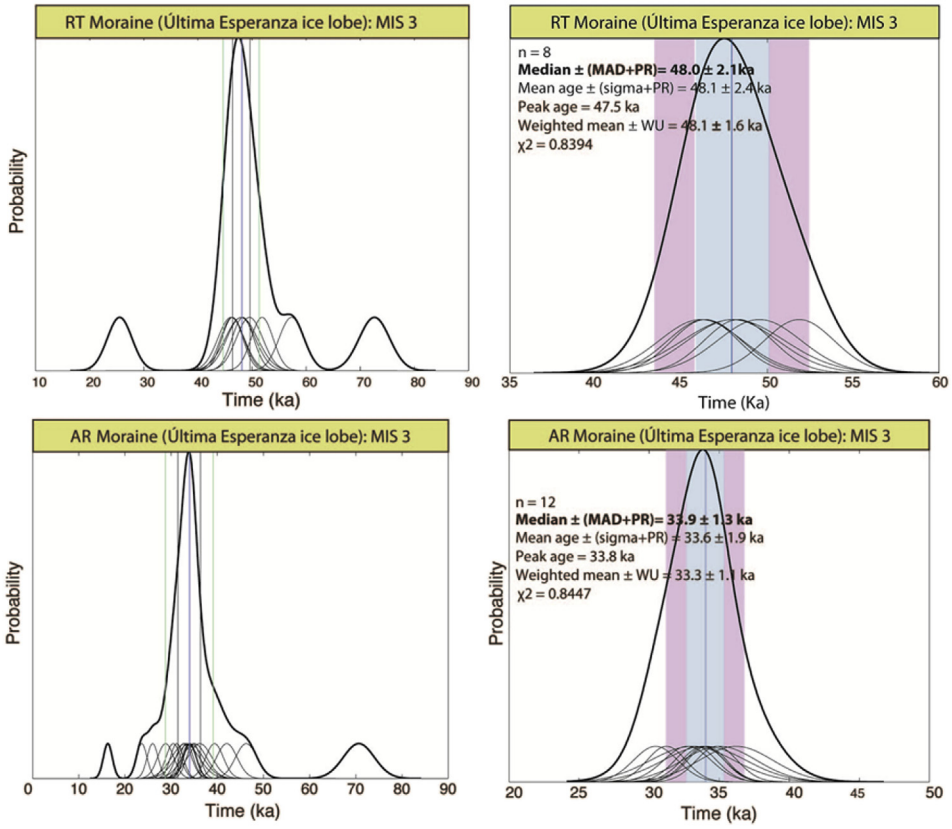

Fig. 6. Probability plots and statistical data for the moraines dated in this study in Última Esperanza. The left plots include all samples and the right plot shows the filtered dataset (i.e., following rejection of outliers) for each moraine. The black and green vertical lines in the left plots indicate the 1 x MAD and 2 x MAD from the median (blue line), respectively. In the right plots, the vertical blue line represents the median age of the moraine. The light blue and pink vertical bands represent the ±1 and 2 uncertainties (MAD + 3% ^{10}Be production rate), respectively, for the filtered moraine. (For interpretation of the references to color in this figure legend, the reader is referred to the Web version of this article.)

northern RT lateral moraine, which yielded a median exposure age of 48.0 ± 2.1 ka (n = 8; age range 46.1 ka − 51.9 ka). The inner AR moraine was also sampled from the northern lateral, but also includes the Sierra Dorotea site. Altogether, the ages from the AR moraine yielded a median exposure-age of 33.9 ± 1.3 ka (n = 12, age range 30.5 ka − 36.2 ka) (Fig. 8).

5. Discussion

5.1. Glacier advances by the Torres del paine and Última Esperanza ice lobes

For the Torres del Paine ice lobe, we interpret the RV I moraine complex to include at least two main glacial advances culminating first at 48.0 ± 1.6 ka (RV I terminal moraine), and then at 39.2 ± 2.0 ka (RV I lateral moraine). A third and a fourth ice advance followed at 35.0 ± 1.5 ka (RV II lateral moraine) and then at 21.5 ± 1.8 ka (TDP I lateral moraine). Within statistical uncertainties, the first and third of these advances were also recorded by the Última Esperanza ice lobe by the Río Turbio moraine deposition at 48.0 ± 2.1 ka, and the Arauco moraine at 33.9 ± 1.3 ka, respectively. We therefore combined the moraine record from both glacial basins and obtained a composite glacial chronology that included 4 glacial advances at 48.0 ± 1.6 ka, 39.2 ± 2.0 ka, 34.0 ± 1.3 ka and 21.5 ± 1.8 ka (Figs. 7–8). Our data suggest that the Torres del Paine and Última Esperanza ice lobes advanced in close synchrony, confirming a correlated response to climate forcing rather than local glacier dynamics.

5.2. The patagonian lLGM

Our data demonstrate a comprehensively dated maximum glacial extent at 48 ± 1.8 ka in Patagonia during MIS 3, about 15 kyr earlier than the previously considered start of the lLGM in the region (cf., Denton, et al., 1999; Kaplan et al., 2008a; Moreno et al., 2015).

The convention in the literature suggests that Patagonian glaciers reached their lLGM between about 29.0 and 17.8 ka (Kaplan et al., 2004, 2008a; Sudgen et al., 2005; McCulloch et al., 2005; Douglass et al., 2006; Hein et al., 2010; Darvill et al., 2016). These studies are based on direct moraine dating using terrestrial cosmogenic nuclides (e.g., ^{10}Be) along the Patagonian Andes. Nonetheless, there is strong evidence for an earlier glacier expansion in southern South America. For instance, in the Chilean Lake District, using a stratigraphic-based approach, Denton et al. (1999), confirmed later by Moreno et al. (2015), dated the lLGM to be between about 33.6 and 17.8 ka, exposing a late MIS 3 expansion to outer moraines at the north Patagonian Andes. Sagredo et al. (2011), based on three ^{10}Be ages from boulders resting on moraines in Última Esperanza, obtained a earlier glacier advance dated to c. 38 ka. A MIS 3 glacier expansion is supported by the study of Darvill et al. (2015a), which suggested two extensive glacial advances at 45.6 (+139.9/−14.3) ka and 30.1 (+45.6/−23.1) ka. Evidence for an early expansion of the PIS during the late MIS 3 has also been suggested from ^{10}Be-dated moraines in the Lago San Martín basin (Glasser et al., 2011). Altogether, glacier chronologies demonstrate that at least during various segments, the MIS 3 was a

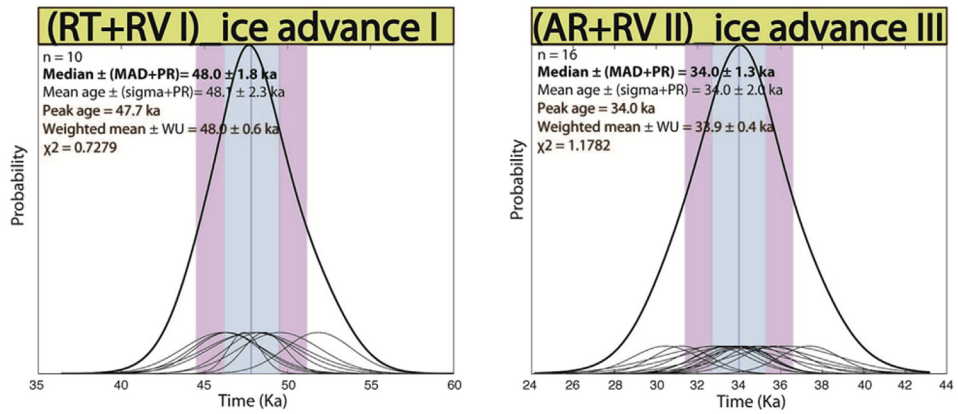

Fig. 7. Probability plots including the combined ^{10}Be ages from the RVI_terminal + RT moraines (left) and RV II + AR moraines (right) and the respective age of the I and III ice advances defined this way in this study.

period of climatic deterioration and extensive ice in Patagonia. This may be in apparent contrast with paleoecological records evidencing MIS 3 interstadial conditions in the Isla de Chiloé at 42°S (Heusser et al., 1999; Roig et al., 2001; Villagrán et al., 2004).

Our data also indicate that the Torres del Paine ice lobe readvanced during the peak of the gLGM at 21.5 ± 1.8 ka, as did Patagonian glaciers elsewhere (e.g., Denton et al., 1999; Kaplan et al., 2008a), but this MIS 2 advance was substantially smaller, reaching just half the eastward extent of the local MIS 3 maximum. Darvill et al. (2015a) reached a similar conclusion, showing that the MIS 3 Río Cullen and San Sebastian glacial advances were significantly greater than the gLGM ice extent in Tierra del Fuego. The implication is that glacial conditions during MIS 3 seems to have been more pronounced than those during the gLGM, at least in southern Patagonia.

Despite robust evidence showing expanded ice during mid MIS 3, there is, as yet, no direct evidence for growth of glaciers during MIS 4 in Patagonia, although this scenario cannot be ruled out. In fact, sea surface temperature (SST) offshore of Patagonia (Kaiser et al., 2005) and, likely, pollen records (Heusser et al., 1999) afford evidence for stadial conditions during MIS 4. These records show either the same or colder conditions during MIS 4 compared to MIS 2, which should have prompted Patagonian glaciers to expand at this time (Denton et al., 1999; Kaplan et al., 2008a). Indeed, dust peaks in Antarctic ice cores that have been linked to glacial activity in Patagonia are also suggestive of heightened

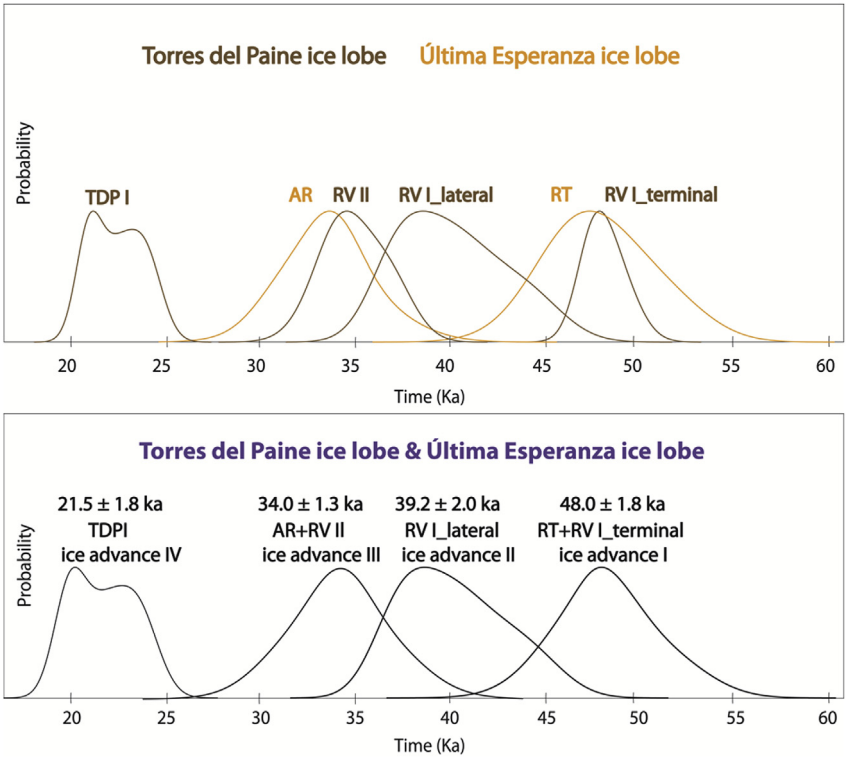

Fig. 8. Glacial advances by the Torres del Paine and Última Esperanza ice lobes as depicted by summed probability plots of moraine ages. All filtered data from this study have been plotted to illustrate the similar ice fluctuations recorded by both glaciers. **Upper panel.** Each peak represents the highest probability for the timing of a glacial advance culmination. **Lower panel.** Combined Torres del Paine and Última Esperanza records that define four distinct ice expansions during the last glacial period.

glacial activity in Patagonia during MIS 4 (Sugden et al., 2009). Rejected outliers presented here and in previous studies (e.g., Sagredo et al., 2011), with ^{10}Be exposure ages between c. 60–70 ka, hint at an early expansion of the Última Esperanza ice lobe to the outer moraine belt during MIS 4.

In our present understanding, the lLGM in Patagonia encompasses multiple (e.g., 6–8) glacial advances that deposited moraine crests as far as c. 100–200 km away from the present ice margins between 48.0 and 17.8 ka. For instance, our study has revealed four glacial advances occurring between c. 48 ka and 21 ka at the Torres del Paine and Última Esperanza basins. At least five other glacial advances between c. 33-18 ka have been recorded at different glacier basins, such as the Strait of Magellan, Bahía Inútil, Lago Pueyrredón, Lago Buenos Aires, or the Chilean Lake District along the Patagonian Andes (e.g., Denton et al., 1999; Kaplan et al., 2004, 2008b; McCulloch et al., 2005; Douglass et al., 2006; Hein et al., 2010; Daevill et al., 2015a). Some of the glacier advances in our study area match, within uncertainties, the timing of previously identified glacial expansions in Patagonia, such as that at c. 33.6 ka in the Chilean Lake District (Denton et al., 1999; Moreno et al., 2015) or that at 45.6 ka (+139.9/−14.3) in Tierra del Fuego (Darvill et al., 2015a), but most of the MIS 2 glacial activity recorded in Patagonia seems not to be preserved in Torres del Paine nor in Última Esperanza, except for the advance at 21.5 ± 1.8 ka.

5.3. The southern middle latitude LGM

At the other side of the Pacific Ocean, the available paleoclimate records for an early (i.e., before MIS 2) New Zealand glaciation linked to cool atmospheric and oceanographic conditions are more widespread than in southern South America (e.g., Preusser et al., 2005; Barrows et al., 2007; McCarthy et al., 2008; Schaefer et al., 2015; Williams et al. 2015). Glaciers of the Southern Alps expanded to reach their maximum extent of the last "Otira" glaciation during MIS 4. For instance, based on many ^{10}Be exposure-dates of boulders embedded in the outermost moraine belt, Schaefer et al. (2015) provided definitive evidence for both the Pukaki and Tekapo glaciers (44 S°) achieving their lLGM by c. 65 ka, building on previous work from the Southern Alps (Fink et al., 2006; Sutherland et al., 2007; McCarthy et al., 2008). Major MIS 3 glacier readvances followed at c. 49-47 ka, c. 42 ka and c. 35–36 ka (Kelley et al., 2014; Schaefer et al., 2015; Doughty et al., 2015; Williams et al., 2015). The glacial expansions occurred along with cooling episodes recorded also by pollen, speleothem $\delta^{18}O_c$, loess and SST proxies described in detail by Williams et al. (2015). For instance, $\delta^{18}O_c$ values from speleothems reveal shifts to negative values indicative of cooling atmospheric trends at 66-64 ka, 49-48 ka and c. 42-38 ka. Similarly, at 67 ka a positive excursion of *G. bulloides* $\delta^{18}O$ values offshore from New Zealand achieved near gLGM levels (Williams et al., 2015).

Excluding MIS 4, a period lacking well constrained evidence for glacial activity in Patagonia, we infer a similar MIS 3 glacial history between Patagonia and New Zealand (e.g., Almond et al., 2001; Shulmeister et al., 2010; Kelley et al., 2014; Doughty et al., 2015). Despite that MIS 3 climate seems to have ameliorated in New Zealand, this period was punctuated by repeated cold stadials that included glacial expansions at least at 49-47 ka and 38–42 ka, and c.35.5 ka in agreement with the geochronologic glacial evidence from the Torres del Paine and Última Esperanza ice lobes. Some of these glacial advances in the Southern Alps extended to just behind the MIS 4 moraines and embraced full glacial conditions such as in our study area (e.g., Kelley et al., 2014). Therefore, the available evidence shows similar MIS 3 glacial histories at both sides of the Pacific and documents a southern mid latitude mountain glacier climate signal. A comparable glacial history between the Patagonian Andes and the Southern Alps of New Zealand also involved MIS 2, with multiple extensive glacial advances culminating between c. 33 ka and 17.5 ka (Denton et al., 1999; Putnam et al., 2013; cf., Williams et al., 2015).

In both mountain chains, the maximum glacial extent predated the gLGM period, either during the MIS 4 or MIS 3. Nonetheless, several southern mountain glaciers do not show such an early glacial maxima record (e.g., Kaplan et al., 2004; Putnam et al., 2013). In such cases, one possibility is that the greater glacial extent during the gLGM overrode earlier glacial expansions at MIS 4 and MIS 3.

5.4. The Antarctic millennial-scale connection

Our data suggest a multi-millennial link between the southern hemisphere mid and high latitude climate changes. The glacial expansions at 48 ± 1.8 ka, 39 ± 2.0 ka, 34.0 ± 1.3 ka and 21.5 ± 1.8 ka by the Torres del Paine and Última Esperanza ice lobes correspond, within uncertainties, to millennial-scale cool phases recorded in Antarctic ice cores (Fig. 9d–e). In other words, the ice advances revealed here culminated in phase within uncertainties with an Antarctic stadial (Blunier and Brook, 2001; Jouzel et al., 2007; WAIS Divide Project Members, 2015). Therefore, taking it at face value, our data show that Patagonian glaciers fluctuated in phase with Antarctic climate not only during the gLGM (e.g., Sugden et al., 2009), but earlier in the glaciation also. If so, glacier advances recorded in this study reveal the sensitivity of low gradient PIS outlet glaciers to c. 2°C Antarctic climate cooling stages that punctuated the last glacial period (Jouzel et al., 2007). Dust peaks as recorded in East Antarctica (Lambert et al., 2012, Fig. 9d) coincide with the advances of the TDP and UE ice lobes and therefore support the view of Patagonia glacial fluctuations controlling the dust flux over East Antarctic during the glacial periods (e.g., Sugden et al., 2009; Kaiser and Lamy, 2010). Stadial conditions in Antarctica were accompanied by Southern Ocean cooling and winter sea ice expansion into lower latitudes (e.g., Mashiotta et al., 1999; Bianchi and Gersonde, 2004, Fig. 9f). A concurrent northward shift of the Antarctic cold water and its deflection along the western coast of southern South America has been recorded as far as 41°S throughout the last glacial period and tied to PIS advances (Lamy et al., 2004; Kaiser et al., 2005; Caniupán et al., 2011) (Fig. 9g). The southern westerly wind belt shifted or expanded north and acted as a main modulator of millennial-scale climate changes intensifying cooling and humid conditions in the mid latitudes during each Antarctic stadial. Therefore, a cooler and wetter atmosphere tied to lower sea surface temperatures and shifted westerlies accompanied and led to the expansion of glaciers in Patagonia (Kohfeld et al., 2013). These linkages between southern glacial expansion and Antarctic cooling have been recorded in New Zealand also, therefore supporting the southern mid-latitude view of glacial fluctuations being in phase with Antarctic climate and Southern Ocean change at millennial timescales throughout the last glacial period (e.g., Lamy et al., 2004, 2015; Sugden et al., 2009; Putnam et al., 2010a; Barrows et al., 2007; García et al., 2012; Strelin et al., 2011; Kelley et al., 2014; Doughty et al., 2015; Caniupán et al., 2011). In addition, North Atlantic Dansgaard Oeschger interstadials coincided with a northern shift of the thermal equator and the southern westerlies linked to the expansion of the Southern Ocean fronts and the Antarctic sea ice margins. The latter expose a potential interhemispheric link between the oceanic and atmospheric bipolar seesaw and ice fluctuations in the south through the last glacial period (Anderson et al., 2009; Denton et al., 2010; García et al., 2012; Darvill et al., 2016).

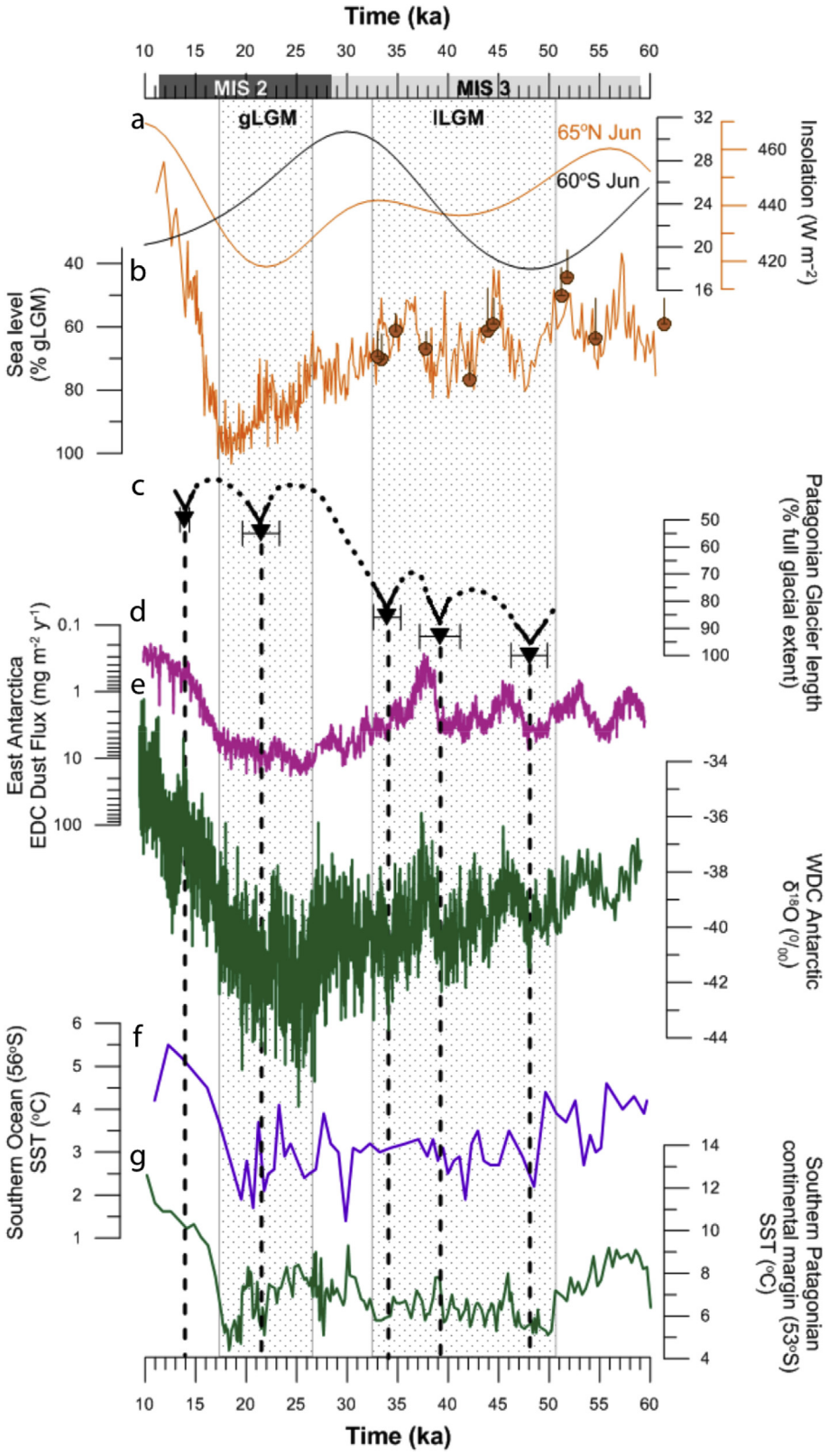

Fig. 9. Paleoclimatic and Paleoceanographic context. a) Insolation intensity for June at 60°S (southern winter, black) and July 65°N (northern summer, orange) (Berger and Loutre, 1991). **b)** Sea level fluctuations expressed as percentages (%) of total change during the last glacial period. The high-resolution curve is the benthic O-isotope record of site MD952042 (Shackleton et al., 2000), which is illustrative of global sea level change modulated by the northern continental ice sheets. Closed circles are the dated corals at Huon Peninsula (Chappell, 2002). Uncertainties shown are 1 standard deviation. **c)** Patagonian glacier advances and ice extent expressed as percentage relative to present ice margin (this study; the younger advance by García et al., 2012). **d)** East Antarctic EPICA Dome C dust flux (Lambert et al., 2012). **e)** West Antarctic Ice Sheet divide ice core O-isotope record (WAIS Divide Project Members, 2015). **f)** E11-2 site (Pacific sector of the Southern Ocean) sea surface temperature (SST) (Mashiotta et al., 1999). **g)** MD07-3128 site (southern Patagonia continental margin, c. 1100 m depth) SST (Caniupán et al., 2011). Grey hatched areas indicate the lLGM: local last glacial maximum based on this study and the gLGM: global last glacial maximum (Mix et al., 2001). (For interpretation of the references to color in this figure legend, the reader is referred to the Web version of this article.)

5.5. The southern insolation role

So far, we have suggested that there is a direct link between Antarctic climate change and southern mid-latitude glacier response at millennial times-scales throughout the last glacial period. We now consider the cause of an early MIS 3 maximum as compared to the MIS 2 glacial extent in Patagonia. We suggest that changes in obliquity-modulated southern winter-insolation may affect long-term fluctuations of the southern PIS (Fig. 9a, c). Insolation effects may be enhanced or reduced by positive or negative feedbacks, respectively, driving the apparent asymmetry of maximum glaciation within the southern latitudes.

The PIS reached its maximum extent of the last glacial period at c. 48 ka in TDP and UE, and likely in Tierra del Fuego (Darvill et al., 2015a). Huybers and Denton (2008) proposed that Antarctic temperature at orbital time scales was controlled by season duration and that this climatic signal propagated its influence to the adjacent southern middle latitudes through coupled sea ice and CO_2 feedbacks. Despite that the maximum at 48 ka occurred when summers were shortening and winters expanding, this trend only lasted a few thousand years and is uncharacteristic for the MIS 3 period, which, in turn, was dominated by long summers and short winters in the south (Huybers and Denton, 2008). Therefore, the duration of seasons doesn't appear to be an obvious control of the PIS maximum in south Patagonia. On-the-other-hand, obliquity-modulated high latitude winter-insolation intensity reached a minimum at about 48 ka (Fig. 9a), coincident with the southern PIS maximum extent at TDP and UE. Therefore, it is possible that orbitally driven winter intensity played a causal role driving the PIS extent fluctuations. Atmospheric cooling (during glacial periods) promotes the Southern Ocean stratification and expanded sea ice (Sigman et al., 2004) at the same time as a northward shift of the Polar Front and intensification of the southern westerlies, and associated southern glacial expansion (cf., Kohfeld et al., 2013). As winter sea-ice is related to Antarctic temperature (Wolff et al., 2006), it could be expected that a minimum in cold winter temperatures during high obliquity coincided with extended winter sea ice, intensified open Southern Ocean stratification, and southern mid-latitude glaciation. In this regard, we suggest that the southern PIS maximum at 48 ka should have been affected by very intense winter conditions, which were caused by a combination of forcings: (1) a long-term high obliquity peak in coincidence with (2) a short-term Antarctic stadial period (Fig. 9a, c-f). In west Antarctica, the stadial culminated at about 48 ka (WAIS Divide Project Members, 2015, Fig. 9e). Possibly, the slight shortening of the summer duration at this time also favored the lLGM. Therefore, both orbital and suborbital phases may have added together to prime a distinct maximum glacial extent as recorded in south Patagonia.

The peak in obliquity at about 48 ka should have produced an intensified seasonality with warmer summers and colder winters. Nonetheless, the peak in southern summer insolation intensity at this time appears not to have prevented the southern PIS reaching a maximum. In this regard, even though high obliquity has been linked to overall unfavorable conditions for glaciation (e.g., Huybers and Wunsch, 2005), we instead observe the maximum southern glacial extent during a period of high obliquity. We point to the maritime condition of the southern hemisphere, particularly at its mid-high latitudes, which permits a reduced seasonality (e.g., mild summers) compared to the northern “continental” hemisphere where high obliquity exacerbates seasonality. The obliquity peak at about 48 ka led to the lowest southern winter insolation within the last glacial period (e.g., not reached during the gLGM), which we suggest favored maximum glacial extent in southern Patagonia. Inboard MIS 3 moraines, such as RV II and AR moraines, were deposited at 34 ka, during warmer winters (Fig. 9a). During the gLGM, when the PIS reached half the extent in TDP, winters were milder than the MIS 3, helping to explain, at least in part, the change in the southern PIS extent through the last glaciation and the potential effect of orbital forcing on mid-latitude southern hemisphere glacier fluctuations.

An aspect of the southern mountain glacial history that we cannot entirely reconcile is why different southern glaciers reached maximum extents at different times within the last glacial period, despite the same putative insolation forcing. In other words, why different southern glaciers seem to expose dissimilar ice extents through the last glacial period (e.g., Kaplan et al., 2004, 2008a,b; Putnam et al., 2013; Schaefer et al., 2015; Darvill et al., 2015a, 2016; this study). Such a scenario could be determined by positive and negative feedbacks enhancing or counteracting the prime insolation forcing. Moreover, considering the extensive latitudinal climatic range of Patagonia and, to a lesser degree, New Zealand, together with the dissimilar local styles of glaciation and topography, a disparity in the ice extent throughout the last glacial period can be expected (i.e., asymmetry of maximum glaciation within one mountain range). In this regard, the ice extent at MIS 4, MIS 3 and MIS 2 in different basins should have been ultimately determined by local-to-regional scale controls, which in turn were superimposed on the rhythm insolation change beat (e.g., Putnam et al., 2013; Doughty et al., 2015; Darvill et al., 2016). Our study exposes that the MIS 2 glaciation was half the extent of the MIS 3 glaciation in TDP. As mentioned above, this could be explained by the milder winters at the gLGM compared to the MIS 3. Nonetheless, it seems that other forcings also applied. For instance, the ice retreat at the end of the MIS 3 into the recorded MIS 2 position (i.e., TDP I moraine in Torres del Paine) could have been enhanced by positive feedbacks, such as breakdown effect of proglacial lakes (García et al., 2014), and/or the snow starvation effect in response to the westward migration of the ice divide (towards the precipitation source) that is suggested to have occurred as the PIS built up, and thus restricting glacier extent to the east during the gLGM (Sugden et al., 2002). In the same manner, the interpreted dry conditions in southern Patagonia in response to a northward migration of the westerlies during the MIS 2 may have also constrained the southern ice extent at this time (Heusser, 1989; Hulton et al., 2002; Kohfeld et al., 2013). This is consistent with indications of a slower Antarctic Circumpolar Current and Drake Passage throughflow during the LGM, most likely together with reduced westerlies, drier southern Patagonia and reduced ice extent (cf., Lamy et al., 2015). Moreover, if the atmospheric and/or oceanic bipolar seesaw ultimately controls the position of the southern westerlies, short-term glacier advances superimposed on long term PIS front variations, could be affected by remote interhemispheric teleconnections (Anderson et al., 2009; Denton et al., 2010). Therefore, our best explanation is that long term insolation change through variation in winter conditions (e.g., embraced by the glacial mode Southern Ocean stratification and sea ice extent; Sigman et al., 2004; Putnam et al., 2013) affects long-term PIS and southern mountain glaciation, which at short time scales can ultimately be forced by regional to local mechanisms that either counteract or enhance the insolation effect. We agree with Doughty et al. (2015) and Darvill et al. (2016) that insolation changes alone cannot explain the timing of glacial advances because these are rather a consequence of millennial scale shifts in the Antarctic and Southern Ocean-atmospheric system, which affected already expanded (i.e., in glacial mode) southern glaciers (cf., Barrows et al., 2007; Lamy et al., 2015).

5.6. Interhemispheric glacial fluctuations

Glacier records suggest that the southern mountain glaciers and

northern ice sheets may have fluctuated out-of-phase during the last glacial period (e.g., Kelley et al., 2014; Schaefer et al., 2015; Fink et al., 2006; Sutherland et al., 2007; McCarthy et al., 2008). The prolonged mild interstadial conditions of MIS 3 identified in the northern hemisphere (e.g., Parducci et al., 2012; Dalton et al., 2016; Ivy-Ochs et al., 2008) were not experienced by southern mountain glaciers, which were at or close to their maximum positions at this time (This study, Doughty et al., 2015; Darvill et al., 2015a; Kelley et al., 2014) (Fig. 9c). Global eustatic sea level, as a proxy for northern continental ice-sheet volume, had reached only near half of the gLGM sea-level lowstand by MIS 3 (Shackleton et al., 2000; Chappell, 2002) (Fig. 9b). Similarly, northern hemisphere MIS 3 interstadial ice-free areas that were later overridden by ice at the gLGM have been recorded for the Alps, the Fenoscandian and the Laurentide ice sheets (Parducci et al., 2012; Dalton et al., 2016; Ivy-Ochs et al., 2008). Therefore, paleoglacier records suggest a lack of agreement in the timing of maximum glaciation extent between northern ice sheets and southern mountain glaciers. This glacier change occurs despite Antarctic and Greenland air temperature changes that appear nearly in-phase at orbital scales during the last glacial cycle (Jouzel et al., 2007; Huybers and Denton, 2008). We believe that the contrasting glacial maxima in opposing hemispheres can be explained in part due to the respective polar insolation changes throughout the last ice age (Fig. 9a). In this scenario, we tentatively suggest that the Earth's orbital configuration during MIS 3 prompted maximum or near maximum glaciation in the south while the orbital configuration during MIS 2 drove maximum continental glaciation in the north (when northern summer insolation intensity was at its lowest) (Berger and Loutre, 1991). The long-term buildup of northern continental ice sheets, as based on sea level reconstructions (e.g., Shackleton et al., 2000; Chappell, 2002, Fig. 9a), largely followed an uninterrupted trend of favorable insolation intensity since late MIS 3, culminating at c. 21 ka during the gLGM. In contrast, southern mountain glaciers, at least those ice lobes in the Sub-Antarctic region, could have responded to a relatively less favorable orbital configuration at this time, and reached a relatively reduced extent compared to earlier in the glaciation. As discussed in the previous section, the northward migration of the westerlies should have intensified the reduced extent of the southern Patagonian glaciers during the gLGM, and thus the inter-hemispheric difference in maximum glaciation.

6. Conclusions

- The Torres del Paine and Última Esperanza ice lobes advanced through the last glaciation at 48.0 ± 1.8 ka, 39.2 ± 2.0 ka, 34.0 ± 1.3 ka and 21.5 ± 1.8 ka.
- The Torres del Paine and Última Esperanza ice lobes reached their maximum extent at 48.0 ± 1.8 ka, which was twice as extensive as the ice extent at 21.5 ± 1.8 ka during the gLGM. The MIS 3 maximum was due to the added effects of (orbitally-driven) southern cold winters and (millennial scale) Antarctic stadial conditions. Less extensive gLGM ice in southern Patagonia coincided with milder winters than during MIS 3, in addition to probable dry conditions affecting the tip of southern South America at this time.
- The glacial maximum in south Patagonia is out-of-phase with the northern continental ice sheets.
- Within statistic uncertainties, each of the glacial advances recorded by this study occurred synchronously with Antarctic stadials. Together, glacier records in Patagonia and New Zealand suggest a consistent ocean, atmosphere and cryosphere, high-to mid-latitude teleconnection, over millennial time scales in the southern hemisphere, probably linked to the North Atlantic throughout the last glacial period.

Acknowledgements

We thank Joerg Schaefer and Michael Kaplan for supporting the preparation of samples RVI-08-01 & RVI-08-02 in LDEO cosmo lab. We thank Juan José Ferrada, Francisca Santana for contributing to this study, and Fabrice Lambert Esteban Sagredo, David Sugden for constructive discussion along this work. We are grateful to Patagonian estancias San Antonio, Cerro Guido, El Palenque, Llanuras de Diana, Dorotea, Laguna Salada and Tapi Aike for providing help and support during fieldwork campaigns. This work was supported by FONDECYT (Grants# 11110381 and # 1161110).

Appendix A. Supplementary data

Supplementary data related to this article can be found at https://doi.org/10.1016/j.quascirev.2018.01.013.

References

Almond, P.C., Moar, N.T., Lian, O.B., 2001. Reinterpretation of the glacial chronology of south Westland, New Zealand. N. Z. J. Geol. Geophys. 44, 1–15. https://doi.org/10.1080/00288306.2001.9514917.

Anderson, R.F., Ali, S., Bradtmiller, L.I., Nielsen, S.H.H., Fleisher, M.Q., Anderson, B.E., Burckle, L.H., 2009. Wind-driven upwelling in the Southern Ocean and the deglacial rise in atmospheric CO2. Science 323, 1443–1448.

Balco, G., Stone, J.O., Lifton, N.A., Dunai, T.J., 2008. A complete and easily accesible means of calculating surface exposure ages or erosion rates from 10Be and 26Al measurements. Quat. Geochronol. 3, 174–195. https://doi.org/10.1016/j.quageo.2007.12.001.

Barrows, T.T., Juggins, S., De Deckker, P., Calvo, E., Pelejero, C., 2007. Long-term sea surface temperature and climate change in the Australian-New Zealand region. Paleoceanography 22, 1–17.

Bendle, J.M., Palmer, A.P., Thorndycraft, V.R., Mathews, I.P., 2017a. The glacial geomorphology of the Lago Buenos Aires and Lago pueyrredon ice lobes of central Patagonia. J. Maps 13, 654–673.

Bendle, J.M., Thorndycraft, V.R., Palmer, A.P., 2017b. High-resolution chronology for deglaciation of the patagonian ice sheet at Lago Buenos Aires (46.5S) revealed through varve chronology and bayesian age modelling. Quat. Sci. Rev. 177, 314–339.

Berger, A., Loutre, M.F., 1991. Insolation values for the climate of the last 10 million years. Quat. Sci. Rev. 10, 297–317. https://doi.org/10.1016/0277-3791(91)90033-Q.

Bianchi, C., Gersonde, R., 2004. Climate evolution at the last deglaciation: the role of the Southern Ocean. Earth Planet Sci. Lett. 228, 407–424. https://doi.org/10.1016/j.epsl.2004.10.003.

Bierman, P.R., Caffee, M.W., Davis, P.T., Marsella, K., Pavich, M., Colgan, P., Mickelson, D., Larsen, J., 2002. Rates and timing of earth surface processes from in situ-produced cosmogenic Be-10. In: Grew, E. (Ed.), Beryllium: Mineralogy, Petrology, and Geochemistry, Reviews in Mineralogy & Geochemistry, vol. 50. Mineralogical Society of America, Washington, pp. 147–205. https://doi.org/10.2138/rmg.2002.50.4.

Binnie, S.A., Dunai, T.J., Voronina, E., Goral, T., Heinze, S., Dewald, A., 2015. Separation of Be and Al for AMS using single-step column chromatography. Nucl. Instrum. Meth. Phys. Res. B 361, 397–401.

Blunier, T., Brook, E.J., 2001. Timing of millennial-scale climate change in Antarctica and Greenland during the last glacial period. Science 291, 109–112. https://doi.org/10.1126/science.291.5501.109.

Broecker, W.S., Denton, G.H., 1989. The role of ocean-atmosphere reorganizations in glacial cycles. Geochem. Cosmochim. Acta 53, 2465–2501. https://doi.org/10.1016/0016-7037(89) 90123–3.

Caldenius, C.C., 1932. Las Glaciaciones Cuaternarias en Patagonia y Tierra del Fuego. Geogr. Ann. 14, 1–164. https://doi.org/10.2307/519583.

Caniupán, M., et al., 2011. Millennial-scale sea surface temperature and Patagonian Ice Sheet changes off southernmost Chile (53°S) over the past ~60kyr. Paleoceanography 26, PA3221. https://doi.org/10.1029/2010PA002049.

Carrasco, J.F., Cassasa, G., Rivera, A., Aniya, M., Naruse, R., 2002. Meteorological and climatological aspects of the southern Patagonia icefield. In: Cassasa, G., Casassa, G., Sepúlveda, F.V., Sinclair, R.M. (Eds.), The Patagonian Icefields. Kluwer Academic/Plenum Publishers, New York, pp. 29–41. https://doi.org/10.1007/978-1-4615-0645-4_4.

Chappell, J., 2002. Sea level forced ice breakouts in the Last Glacial cycle: new results from corals. Quat. Sci. Rev. 21, 1229–1240. https://doi.org/10.1016/S0277-3791(01)00141-X.

Dalton, A.S., Finkelstein, S.A., Barnett, P.J., Forman, S.L., 2016. Constraining the late pleistocene history of the Laurentide ice sheet by dating the missinaibi formation, hudson bay lowlands, Canada. Quat. Sci. Rev. 146, 288–299. https://doi.org/10.1016/j.quascirev.2016.06.015.

Darvill, C.M., Stokes, C.R., Bentley, M.J., Lovell, H., 2014. A glacial geomorphological map of the southernmost ice lobes of Patagonia: the Bahía Inútil – san

sebastián, magellan, otway, skyring and Río gallegos lobes. J. Maps 10, 500–520. https://doi.org/10.1080/17445647.2014.890134.
Darvill, C.M., Bentley, M.J., Stokes, C.R., Hein, A.S., Rodés, A., 2015a. Extensive MIS 3 glaciation in southernmost Patagonia revealed by cosmogenic nuclide dating of outwash sediments. Earth Planet Sci. Lett. 429, 157–169. https://doi.org/10.1016/j.epsl.2015.07.030.
Darvill, C.M., Bentley, M.J., Stokes, C.R., 2015b. Geomorphology and weathering characteristics of erratic boulder trains on Tierra del Fuego, southernmost South America: implications for dating of glacial deposits. Geomorphology 228, 382–397.
Darvill, C.M., Bentley, M.J., Stokes, C.R., Shulmeister, J., 2016. The timing and cause of glacial advances in the southern mid-latitudes during the last glacial cycle based on a synthesis of exposure ages from Patagonia and New Zealand. Quat. Sci. Rev. 149, 200–214.
Darvill, C.M., Stokes, C.R., Bentley, M.J., Evans, D.J.A., Lovell, H., 2017. Dynamics of former ice lobes of the southernmost Patagonian Ice Sheet based on a glacial landsystems approach. J. Quat. Sci. 32, 857–876.
Denton, G.H., Heusser, C.J., Lowell, T.V., Moreno, P.I., Andersen, B.G., Heusser, L.E., Schlu̇chter, C., Marchant, D.R., 1999. Interhemispheric linkage of paleoclimate during the last glaciation. Geogr. Ann. 81 A, 107–153. https://doi.org/10.1111/1468-0459.00055.
Denton, G.H., Anderson, R.F., Toggweiler, J.R., Edwards, R.L., Schaefer, J.M., Putnam, A.E., 2010. The last glacial termination. Science 328, 1652–1656.
Desilets, D., Zreda, M., 2003. Spatial and temporal distribution of secondary cosmic-ray nucleon intensities and applications to in-situ cosmogenic dating. Earth Planet Sci. Lett. 206, 21–42. https://doi.org/10.1016/S0012-821X(02)01088-9.
Dewald, A., Heinze, S., Jolie, J., Zilges, A., Dunai, T., Rethemeyer, J., Melles, M., Staubwasser, M., Kuczewski, B., Richter, J., Radtke, U., von Blanckenburg, F., Klein, M., 2013. CologneAMS, a dedicated center for accelerator mass spectrometry in Germany. In: Nuclear Instruments and Methods in Physics Research Section B: Beam Interactions with Materials and Atoms, vol. 294, pp. 18–23.
DGA, 1987. Balance Hídrico de Chile. Dirección General de Aguas, Santiago, Chile.
Doughty, A.M., Schaefer, J.M., Putnam, A.E., J.M, Denton, G.H., Kaplan, M.R., Barrell, D.J.A., Andersen, B.G., Kelley, S.E., Finkel, R.C., Schwartz, R., 2015. Mismatch of glacier extent and summer insolation in Southern Hemisphere mid-latitudes. Geology 43, 407–410. https://doi.org/10.1130/G36477.1.
Douglass, D.C., Singer, B.S., Kaplan, M.R., Mickelson, D.M., Caffee, M.W., 2006. Cosmogenic nuclide surface exposure dating of boulders on last-glacial and late-glacial moraines, Lago Buenos Aires, Argentina: interpretive strategies and paleoclimate implications. Quat. Geochronol. 1, 43–58. https://doi.org/10.1016/j.quageo.2006.06.001.
Dunai, T.J., 2001. Influence of secular variation of the magnetic field on production rates of in situ produced cosmogenic nuclides. Earth Planet Sci. Lett. 193, 197–212. https://doi.org/10.1016/S0012-821X(01)00503-9.
Escobar, F., Vidal, F., Garin, C., Naruse, R., 1992. Water balance in the Patagonia icefield. In: Naruse, R., Aniya, M. (Eds.), Glaciological Researches in Patagonia, 1990. Japanese Society of Snow and Ice, pp. 109–119.
Fink, D., Williams, P.W., Augustinus, P., Shulmeister, J., 2006. Glacial chronologies across southern hemisphere latitudes during the past 30 ka and correlations to Antarctic ice cores. In: Burge, P.I., Shulmeister, J., Turney, C. (Eds.), Australasian INTIMATE Meeting. University of Auckland, pp. 14–16.
García, J.L., 2012. Late Pleistocene ice fluctuations and glacial geomorphology of the Archipiélago de Chiloé, southern Chile. Geogr. Ann. 94, 459–479. DOI: 10.1111/j.1468-0459.2012.00471.x.
García, J.L., Kaplan, M.R., Hall, B.H., Schaefer, J.M., Vega, R.V., Schwartz, R., Finkel, R., 2012. Glacier expansion in southern Patagonia throughout the Antarctic cold reversal. Geology 40, 859–862. https://doi.org/10.1130/G33164.1.
García, J.L., Hall, B.L., Kaplan, M.R., Vega, R.M., Strelin, J.A., 2014. Glacial geomorphology of the Torres del Paine region (southern Patagonia): implications for glaciation, deglaciation and paleolake history. Geomorphology 204, 599–616. https://doi.org/10.1016/j.geomorph.2013.08.036.
Garreaud, R.D., 2007. Precipitation and circulation covariability in the extratropics. J. Clim. 20, 4789–4797. https://doi.org/10.1175/JCLI4257.1.
Gersonde, R., Crosta, X., Abelmann, A., Armand, L., 2005. Sea-surface temperature and sea ice distribution of the Southern Ocean at the EPILOG Last Glacial Maximum—a circum-Antarctic view based on siliceous microfossil records. Quat. Sci. Rev. 24, 869–896. https://doi.org/10.1016/j.quascirev.2004.07.015.
Gillespie, A., Molnar, P., 1995. Asynchronous maximum advances of mountain and continental glaciers. Rev. Geophys. 33, 311–364. https://doi.org/10.1029/95RG00995.
Glasser, N.F., Jansson, K.N., 2005. Fast-flowing outlet glaciers of the last glacial maximum patagonian icefield. Quat. Res. (Tokyo) 63, 206–211. https://doi.org/10.1016/j.yqres.2004.11.002.
Glasser, N.F., Jansson, K., Harrison, S., Kleman, J., 2008. The glacial geomorphology and Pleistocene history of southern South America between 38 S and 56 S. Quat. Sci. Rev. 27, 365–390. https://doi.org/10.1016/j.quascirev.2007.11.011.
Glasser, N.F., Jansson, K.N., Goodfellow, B.W., de Angelis, H., Rodnight, H., Rood, D.H., 2011. Cosmogenic Nuclide Exposure Ages for Moraines in the Lago San Martin Valley, vol. 75. Quaternary Research, Argentina, pp. 636–646.
Hein, A.S., 2009. Quaternary Glaciations in the Lago Pueyrredón Valley, Argentina [Ph.D. thesis]. University of Edinburgh, Edinburgh.
Hein, A.S., Hulton, N.R.J., Dunai, T.J., Sugden, D.E., Kaplan, M.R., Xu, S., 2010. The chronology of the last glacial maximum and deglacial events in central argentine Patagonia. Quat. Sci. Rev. 29, 1212–1227. https://doi.org/10.1016/j.quascirev.2010.01.020.
Hollin, J.T., Schilling, D.H., 1981. Mountain glaciers and small ice caps. In: Denton, G.H., Hughes, T.J. (Eds.), The Last Great Ice Sheets. Wiley, New York, pp. 179–206. https://doi.org/10.2307/3673075.
Heusser, C.J., 1989. Southern westerlies during last glacial maximum. Quat. Res. 31, 423–425. https://doi.org/10.1016/0033-5894(89)90049-5.
Heusser, C.J., Heusser, L.E., Lowell, T.V., 1999. Paleo- ecology of the southern Chilean Lake District- Isla Grande de Chiloé during middle-Late Llanquihue glacia- tion and deglaciation. Geogr. Ann. 81A, 231–284. https://doi.org/10.1111/1468-0459.00058.
Hughes, P.D., Gibbard, P.L., Ehlers, J., 2013. Timing of glaciation during the last glacial cycle: evaluating the concept of a global "Last Glacial Maximum". Earth Sci. Rev. 125, 171–198. https://doi.org/10.1016/j.earscirev.2013.07.003.
Hulton, N.R.J., Purves, R.S., McCulloch, R.D., Sugden, D.E., Bentley, M.J., 2002. The last glacial maximum and deglaciation in Southern South America. Quat. Sci. Rev. 21, 233–241. https://doi.org/10.1016/S0277-3791(01)00103-2.
Huybers, P., Wunsch, C., 2005. Obliquity pacing of the late Pleistocene glacial terminations. Nature 434, 491–494.
Huybers, P., Denton, G.H., 2008. Antarctic temperature at orbital timescales controlled by local summer duration. Nat. Geosci. 1, 787–792. https://doi.org/10.1038/ngeo311.
Ivy-Ochs, S., Kerschner, H., Reuther, A., Preusser, F., Heine, K., Maisch, M., Kubik, P.W., Schluchter, C., 2008. Chronology of the last glacial cycle in the European Alps. J. Quat. Sci. 23, 559–573. https://doi.org/10.1002/jqs.1202.
Jouzel, J., et al., 2007. Orbital and millennial Antarctic climate variability over the past 800,000 years. Science 317, 793–796. https://doi.org/10.1126/science.1141038.
Kaiser, J., Lamy, F., Hebbeln, D., 2005. A 70-kyr sea surface temperature record off southern Chile (Ocean Drilling Program Site 1233). Paleoceanography 20, PA4009. https://doi.org/10.1029/2005PA001146.
Kaiser, J., Lamy, F., 2010. Links between Patagonian Ice Sheet fluctuations and Antarctic dust variability during the last glacial period (MIS 4-2). Quat. Sci. Rev. 29, 1464–1471.
Kaplan, M.R., Ackert, R.P., Singer, B.S., Douglass, D.C., Kurz, M.D., 2004. Cosmogenic nuclide chronology of millennial-scale glacial advances during O-isotope stage 2 in Patagonia. Geol. Soc. Am. Bull. 116, 308–321. https://doi.org/10.1130/B25178.1.
Kaplan, M.R., Moreno, P.I., Rojas, M., 2008a. Glacial dynamics in southernmost South America during Marine Isotope Stage 5e to the Younger Dryas chron: a brief review with a focus on cosmogenic nuclide measurements. J. Quat. Sci. 23, 649–658. https://doi.org/10.1002/jqs.1209.
Kaplan, M.R., Fogwill, C.J., Sugden, D.E., Hulton, N., Kubik, P.W., Freeman, S., 2008b. Southern patagonian glacial chronology for the last glacial period and implications for Southern Ocean climate. Quat. Sci. Rev. 27, 284–294. https://doi.org/10.1016/j.quascirev.2007.09.013.
Kaplan, M.R., Strelin, J.A., Schaefer, J.M., Denton, G.H., Finkel, R.C., Schwartz, R., Putnam, A.E., Vandergoes, M.J., Goehring, B.M., Travis, S.G., 2011. In-situ cosmogenic 10Be production rate at Lago Argentino, Patagonia: implications for late-glacial climate chronology. Earth Planet Sci. Lett. 309, 21–32. https://doi.org/10.1016/j.epsl.2011.06.018.
Kelley, S.E., Kaplan, M.R., Schaefer, J.M., Andersen, B.G., Barrell, D.J.A., Putnam, A.E., Denton, G.H., Schwartz, R., Finkel, R.C., Doughty, A.M., 2014. High-precision ^{10}Be chronology of moraines in the Southern Alps indicates synchronous cooling in Antarctica and New Zealand 42,000 years ago. Earth Planet Sci. Lett. 405, 194–206. https://doi.org/10.1016/j.epsl.2014.07.031.
Kohfeld, K.E., Graham, R.M., de Boer, A.M., Sime, L.C., Wolff, E.W., Le Quéré, C., Bopp, L., 2013. Southern Hemisphere westerly wind changes during the Last Glacial Maximum: paleo-data synthesis. Quat. Sci. Rev. 68, 76–95.
Kohl, C.P., Nishiizumi, K., 1992. Chemical isolation of quartz for measurement of insitu-produced cosmogenic nuclides. Geochem. Cosmochim. Acta 56, 3583–3587. https://doi.org/10.1016/0016-7037(92)90401-4.
Lamy, F., Kaiser, J., Ninnemann, U., Hebbeln, D., Arz, H.W., Stoner, J., 2004. Antarctic timing of surface water changes off Chile and patagonian ice sheet response. Science 304, 1959–1962. https://doi.org/10.1126/science.1097863.
Lamy, F., Arz, H.W., Kilian, R., Lange, C.B., Lembke-Jene, L., Wengler, M., Kaiser, J., 39 Baeza-Urrea, O., Hall, I.R., Harada, N., Tiedemann, R., 2015. Glacial reduction and millennial scale variations in Drake Passage throughflow. Proc. Natl. Acad. Sci. U. S. A 112, 13496–13501. https://doi.org/10.1073/pnas.1509203112.
Lal, D., 1991. Cosmic ray labeling of erosion surfaces: in-situ nuclide production rates and erosion models. Earth Planet Sci. Lett. 104, 424–439. https://doi.org/10.1016/0012-821X(91)90220-C.
Lambert, F., Bigler, M., Steffensen, J.P., Hutterli, M., Fischer, H., 2012. Centennial mineral dust variability in high-resolution ice core data from Dome C, Antarctica. Clim. Past 8, 609–623. https://doi.org/10.5194/cp-8-609-2012.
Lifton, N., Smart, D., Shea, M., 2008. Scaling time-integrated in situ cosmogenic nuclide production rates using a continuous geomagnetic model. Earth Planet Sci. Lett. 268, 190–201. https://doi.org/10.1016/j.epsl.2008.01.021.
Lifton, N., Sato, T., Dunai, T., 2014. Scaling in situ produced cosmo genie nuclide production rates using analytical approximations to atmospheric cosmic ray fluxes. Earth Planet Sci. Lett. 386, 149–160.
Lisiecki, L.E., Raymo, M.E., 2005. A Pliocene-Pleistocene stack of 57 globally distributed benthic δ^{18}O records'. Paleoceanography 20, PA1003. https://doi.org/10.1029/2004PA001071.
Marden, C.J., Clapperton, C.M., 1995. Fluctuations of the south patagonian icefield during the last glaciation and the holocene. J. Quat. Sci. v.10, 197–210. https://doi.org/10.1002/jqs.3390100302.

Mashiotta, T.A., Lea, D.W., Spero, H.J., 1999. Glacial –interglacial changes in Subantarctic sea surface temperature and delta O-18-water using foraminiferal Mg. Earth Planet Sci. Lett. 170, 417–432. https://doi.org/10.1016/S0012–821X(99)00116-8.

McCarthy, A., Mackintosh, A., Rieser, U., Fink, D., 2008. Mountain glacier chronology from Boulder Lake, New Zealand, indicates MIS 4 and MIS 2 ice advances of similar extent. Arctic Antarct. Alpine Res. 40, 695–708. https://doi.org/10.1657/1523-0430(06-111)[MCCARTHY]2.0.CO;2.

McCulloch, R., Fogwill, C., Sudgen, D., Bentley, M., Kubik, P., 2005. Chronology of the last glaciation in central Strait of magellan and Bahía Inútil, southernmost South America. Geogr. Ann. 87A (2), 289–312. https://doi.org/10.1111/j.0435-3676.2005.00260.x.

Meglioli, A., 1992. Glacial geology and chronology of Southernmost Patagonia and Tierra del Fuego, Argentina and Chile [PhD Thesis]. Lehigh University, Pennsylvania, 215 pp.

Mercer, J., 1984. Simultaneous climatic change in both hemispheres and similar bipolar warming. In: Hansen, J.E., Takahashi, T. (Eds.), Climate Processes and Climate Sensitivity, vol. 29. American Geophysical Union, pp. 307–313. https://doi.org/10.1029/GM029p0307. Geophysical Monograph.

Michel, J., Baumgartner, L., Putlitz, B., Schaltegger, U., Ovtcharova, M., 2008. Incremental growth of the Patagonian Torres del Paine laccolith over 90 k.y. Geology 36, 459–462. https://doi.org/10.1130/G24546A.1.

Milankovitch, M., 1941. Kanon der Erdbestrahlung und seine Andwendung auf das Eiszeitenproblem. Royal Serbian Academy, Belgrade.

Miller, A., 1976. The climate of Chile. In: W (Ed.), Schwerdtfeger, Climates of Central and SouthAmerica, vol. 12. Amsterdam Elsevier, pp. 113–145. World Survey of Climatology.

Mifsud, Ch, Fujioka, T., Fink, D., 2013. Extraction and purification of quartz in rock using hot phosphoric acid for *in situ* cosmogenic exposure dating. Nucl. Instrum. Meth. Phys. Res. B 294, 203–207. https://doi.org/10.1016/j.nimb.2012.08.037.

Mix, A.C., Bard, E., Schneider, R., 2001. Environmental processes of the ice age: land, oceans, glaciers (EPILOG). Quat. Sci. Rev. 20, 627–657. https://doi.org/10.1016/S0277-3791(00)00145-1.

Moreno, P.I., Kaplan, M.R., François, J.P., Villa-Martínez, R., Moy, C.M., Stern, C.R., Kubik, P.W., 2009. Renewed glacial activity during the Antarctic Cold Reversal and persistence of cold conditions until 11.5 ka in SW Patagonia. Geology 37, 375–378.

Moreno, P.I., Denton, G.H., Moreno, H., Lowell, T.V., Putnam, A.E., Kaplan, M.R., 2015. Radiocarbon chronology of the last glacial maximum and its termination in northwestern Patagonia. Quat. Sci. Rev. 122, 233–249. https://doi.org/10.1016/j.quascirev.2015.05.027.

Nishiizumi, K., Imamura, M., Caffee, M.W., Southon, J.R., Finkel, R.C., McAninch, J., 2007. Absolute calibration of Be-10 AMS standards. Nucl. Instrum. Methods Phys. Res., Sect. B 258, 403–413. https://doi.org/10.1016/j.nimb.2007.01.297.

Parducci, L., et al., 2012. Glacial survival of boreal trees in northern scandinavia. Science 335, 1083–1086. https://doi.org/10.1126/science.1216043.

Putnam, A.E., Denton, G.H., Schaefer, J.M., Barrell, D.J.A., Andersen, B.G., Finkel, R.C., Schwartz, R., Doughty, A.M., Kaplan, M.R., Schluchter, C., 2010a. glacier advance in southern middle-latitudes during the antarctic cold reversal. Nat. Geosci. 3, 700–704. https://doi.org/10.1038/ngeo962.

Putnam, A., Schaefer, J., Barrell, D.J.A., Vandergoes, M., Denton, G.H., Kaplan, M., Finkel, R.C., Schwartz, R., Goehring, B.M., Kelley, S., 2010b. In situ cosmogenic ^{10}Be production-rate calibration from the Southern Alps, New Zealand. Quat. Geochronol. 5, 392–409. https://doi.org/10.1016/j.quageo.2009.12.001.

Putnam, A.E., Schaefer, J.M., Denton, G.H., Barrell, D.J.A., Birkel, S.D., Andersen, B.G., Kaplan, M.R., Finkel, R.C., Schwartz, R., Doughty, A.M., 2013. The last glacial maximum at 44°S documented by a ^{10}Be moraine chronology at lake ohau, southern Alps of New Zealand. Quat. Sci. Rev. 62, 114–141. https://doi.org/10.1016/j.quascirev.2012.10.034.

Pigati, J.S., Lifton, N.A., 2004. Geomagnetic effects on time-integrated cosmogenic nuclide production with emphasis on in situ 14C and 10Be. Earth Planet Sci. Lett. 226, 193–205. https://doi.org/10.1016/j.epsl.2004.07.031.

Preusser, F., Andersen, B.G., Denton, G.H., Schluechter, C., 2005. Luminescence chronology of late pleistocene glacial deposits in north Westland, New Zealand. Quat. Sci. Rev. 24, 2207–2227.

Rivera, A., Acuña, C., Casassa, G., Bown, F., 2002. Use of remotely sensed and field data to estimate the contribution of Chilean glaciers to eustatic sea-level rise. Ann. Glaciol. 34, 367–372. https://doi.org/10.3189/172756402781817734.

Roig, F.A., Le-Quesne, C., Boninsegna, J.A., Briffa, K.R., Lara, A., Grudd, H., Jones, P.D., Villagrán, C., 2001. Climate variability 50,000 years ago in mid-latitude Chile as reconstructed from tree rings. Nature 410, 567–570.

Rock, N.M.S., Webb, J.A., McNaughton, N.J., Bell, G.D., 1987. Nonparametric estimation of averages and errors for small data-sets in isotope geoscience: a proposal. Chem. Geol. Isot. Geosci. 66 (1–2), 163–177.

Sagredo, E.A., Moreno, P.I., Villa-Martinez, R., Kaplan, M.R., Kubik, P.W., Stern, C.R., 2011. Fluctuations of the Última Esperanza ice lobe (52°S), Chilean Patagonia, during the last glacial maximum and termination 1. Geomorphology 125, 92–108. https://doi.org/10.1016/j.geomorph.2010.09.007.

Schaefer, J.M., et al., 2015. The southern glacial maximum 65,000 years ago and its unfinished termination. Quat. Sci. Rev. 114, 52–60. https://doi.org/10.1016/j.quascirev.2015.02.009.

Shackleton, N.J., Hall, M.A., Vincent, E., 2000. Phase relationships between millennial-scale events 64,000-24,000 years ago. Paleoceanography 15, 565–569. https://doi.org/10.1029/2000PA000513.

Sigman, D.M., Jaccard, S.L., Haug, G.H., 2004. Polar ocean stratification in a cold climate. Nature 428 (6978), 59–63. https://doi.org/10.1038/nature02357.

Shulmeister, J., Thackray, G.D., Rieser, U., Hyatt, O.M., Rother, H., Smart, C.C., Evans, D.J.A., 2010. The stratigraphy, timing and climatic implications of glaciolacustrine deposits in the middle Rakaia Valley, South Island, New Zealand. Quat. Sci. Rev. 29, 2362–2381. https://doi.org/10.1016/j.quascirev.2010.06.004.

Stone, J.O., 2000. Air pressure and cosmogenic isotope production. J. Geophys. Res. 105, 23753–23759. https://doi.org/10.1029/2000JB900181.

Strelin, J.A., Denton, G.H., Vandergoes, M.J., Ninnemann, U.S., Putnam, A.E., 2011. Radiocarbon chronology of the late-glacial puerto bandera moraines, southern patagonian icefield, Argentina. Quat. Sci. Rev. 30, 2551–2569. https://doi.org/10.1016/j.quascirev.2011.05.004.

Sutherland, R., Kim, K., Zondervan, A., McSaveney, M., 2007. Orbital forcing of mid-latitude Southern Hemisphere glaciation since 100 ka inferred from cosmogenic nuclide ages of moraine boulders from the Cascade Plateau, southwest New Zealand. Geol. Soc. Am. Bull. 119 (3/4), 443–451. https://doi.org/10.1130/B25852.1.

Sugden, D.E., Hulton, N.R., Purves, R.S., 2002. Modelling the inception of the Patagonian icesheet. Quat. Int. 95–96, 55–64.

Sugden, D.E., Bentley, M.J., Fogwill, C.J., Hulton, N.R.J., McCulloch, R.D., Purves, R.S., 2005. Late-glacial glacier events in southernmost South America: a blend of 'northern' and 'southern' hemispheric climatic signals? Geogr. Ann. 87A, 273–288. https://doi.org/10.1111/j.0435-3676.2005.00259.x.

Sugden, D.E., McCulloch, R.D., Bory, A.J.-M., Hein, A.S., 2009. Influence of Patagonian glaciers on Antarctic dust deposition during the last glacial period. Nat. Geosci. 2, 281–285. https://doi.org/10.1038/ngeo474.

Villagrán, C., León, A., Roig, F.A., 2004. Paleodistribución del alerce y ciprés de las Guaitecas durante periodos interestadiales de la Glaciación Llanquihue: provincias de Llanquihue y Chiloé, región de los Lagos, Chile. Rev. Geol. Chile 31 (1), 133–151.

WAIS Divide Project Members, 2015. Precise interpolar phasing of abrupt climate change during the last ice age. Nature 520, 661–665. https://doi.org/10.1038/nature14401.

Warren, C.R., Sugden, D.E., 1993. The Patagonian icefields: a glaciological review. Arct. Alp. Res. 25, 316–331. https://doi.org/10.2307/1551915.

Williams, P.W., McGlone, M., Neil, H., Zhao, J.-X., 2015. A review of New Zealand palaeoclimate from the last interglacial to the global last glacial maximum. Quat. Sci. Rev. 110, 92–106.

Wolff, E.W., et al., 2006. Southern Ocean sea-ice extent, productivity and iron flux over the past eight glacial cycles. Nature 440, 491–496.